Journal of Inorganic Biochemistry 206 (2020) 111019

Contents lists available at ScienceDirect

Journal of Inorganic Biochemistry

journal homepage: www.elsevier.com/locate/jinorgbio

Transition metal complexes with a novel guanine-based (E)-2-(2-(pyridin-2-ylmethylene)hydrazinyl)quinazolin-4(3H)-one: Synthesis, characterization, interaction with DNA and albumins and antioxidant activity

Marialena Lazou[a], Alketa Tarushi[a], Panagiotis Gritzapis[b], George Psomas[a,*]

[a] Laboratory of Inorganic Chemistry, Department of Chemistry, Aristotle University of Thessaloniki, GR-54124 Thessaloniki, Greece
[b] Laboratory of Organic, Bioorganic and Natural Product Chemistry, Molecular Biology and Genetics Department, Democritus University of Thrace, University Campus, Dragana, 68100, Alexandroupolis, Greece

ARTICLE INFO

Keywords:
Quinazolinone
Metal complexes
DNA-binding
DNA-cleavage
Albumin-binding
Antioxidant activity

ABSTRACT

A novel guanine-inspired 2-hydrazinyl-4(3H)-quinazolinone derivative (HL) has been synthesized and characterized. The reaction of HL with Cu(II) in a 1:1 M:L ratio and with Cu(II), Ni(II) and Zn(II) in a 1:2 M:L ratio resulted in the formation of complexes, $[Cu(L)(H_2O)_2](NO_3)$, **1** and $[M(L)_2]$ (M = Cu for **2**, Ni for **3** and Zn for **4**), respectively. In all these complexes, the ligand L is tridentately bound to the corresponding metal. The affinity of the complexes for calf-thymus DNA was examined by diverse techniques and the complexes can intercalate between the DNA-bases. The cleavage ability of the complexes towards supercoiled circular pBR322 plasmid DNA was examined *via* agarose gel electrophoresis experiments in the absence or presence of UVA, UVB or visible light and the DNA-cleavage was found to depend on the concentration and light wavelength used. The binding of the complexes for bovine and human serum albumins was also investigated in order to determine the binding constants and the binding subdomain. The scavenging activity of the compounds was evaluated towards free radicals 1,1-diphenyl-picrylhydrazyl and 2,2′-azinobis-(3-ethylbenzothiazoline-6-sulfonic acid).

1. Introduction

Quinazolinone is considered a privileged scaffold since its moieties may serve as substrate for more than one enzymic targets [1,2]. Quinazolinone derivatives have shown noteworthy biological properties including antimicrobial, antifungal, antimalarial, anti-inflammatory, antiviral, cytotoxic and antiangiogetic activities [3]. It should be noted that the quinazolinone privileged scaffold exists in commercially available drugs [3], such as etaqualone and methaqualone (used as nervous system depressant and hypnotics), nolatrexed (as thymidylate synthase inhibitor and anticancer agent), the antifungal albaconazole, diproqualone (used as anxiolytic, analgesic and antihistaminic agent) and the anti-inflammatory agents fluproquazone and proquazone [3–7].

Among the synthesized quinazolinone derivatives, the Schiff bases have a prevailing position, since diverse such compounds have been designed, isolated, characterized and evaluated for their analgetic and anti-inflammatory properties [8,9], and antimicrobial and antifungal activity [10]. Especially for a series of Schiff bases of quinazoline-4(3H)-one, the structure and biological properties of diverse transition metal complexes have been reported; a series of Cu(II), Co(II), Ni(II), Mn(II), Zn(II) and Cd(II) complexes have shown antimicrobial activity and DNA-cleavage efficacy [11], Ru(II) complexes have shown antibacterial, antineoplastic and cytotoxic activity [12], and Pd(II) [13] and Sn(IV) [14] complexes have exhibited antimicrobial activity and DNA-intercalation potency.

Copper and zinc are among the most important essential trace elements, while the biological relevance nickel has recently gained increasing attention. Copper in human body is involved in diverse human physiological functions including the development of connective tissues, bones and nerve coverings, and it participates in many redox metalloenzymes, such as Cu−Zn superoxide dismutase (SOD) [15,16]. From the medicinal point of view, a result of the bacteriostatic activity of copper is its use for dyes on manufacturing doorknobs and touch surfaces used in hospitals and healthcare settings, so that the growth and transfer of bacteria are inhibited [17], while the copper(II) complex "Casiopeinas®" is in clinical trials as a potential anticancer agent [18]. In the literature, copper compounds have been tested *in vitro* for a

* Corresponding author.
E-mail address: gepsomas@chem.auth.gr (G. Psomas).

https://doi.org/10.1016/j.jinorgbio.2020.111019
Received 19 December 2019; Received in revised form 20 January 2020; Accepted 4 February 2020
Available online 06 February 2020
0162-0134/

variety of potential activities, including anticancer, antimicrobial and antioxidant among others [19–22].

Zinc is an abundant biometal and it is involved in the active center of more than 200 functional proteins [23,24]. Besides the use of zinc compounds in the treatment of skin infections and injuries and other infections responsible for children mortality in Asian and African countries with "Baby Zinc" [25], zinc complexes have been examined for their *in vitro* potential antidiabetic [26], anti-inflammatory [27], antibacterial [28], radical scavenging [29] and antiproliferative [30] activity.

The biological role of nickel is still being recognized despite some known negative effects [31–34]. Urease is the most important nickel metalloprotein [35]. In the context of searching novel metal-based drugs, selected nickel complexes have shown *in vitro* noteworthy antibacterial [36,37], antifungal [38], anti-inflammatory [39], antioxidant [40,41], and antiproliferative [42,43] activity.

DNA is recognized as one of the most common biological targets of anticancer drugs, since one of the main mechanisms of action of the anticancer drugs it the damage of DNA, especially of cancer cells [44]. The reasons of DNA-targeting on cancer therapy are: (i) the gene mutations occurring in the DNA of tumor cells resulting in DNA-alterations, (ii) the differences of DNA-life cycle between normal and tumor cells, and (iii) the higher DNA-replication rate and the lack of repair mechanism of tumor cells [44]. It is important to study the interactions of small molecules with DNA in order to predict possible resultant therapeutic effects; therefore, DNA-binding is usually studied as a preliminary therapeutic approach to cancer treatment [44]. In general, the interaction mode between metal complexes and DNA depends also on the structure of the complexes and their stability. Metal complexes may bind to DNA covalently (when labile group(s) of the complex may be replaced by DNA-bases) or they may interact noncovalently (*via* intercalation, groove-binding or electrostatically) and/or may induce DNA-cleavage [45–48]. It should be noted that the existence of one DNA-binding mode may not prevent the presence of another one and sometimes a single compound may interact with DNA with more than one binding fashions, e.g. intercalation and covalent binding [44]. Furthermore, DNA is also considered as possible target of photodynamic therapy, and the alterations of DNA-binding induced by irradiation are also of increasing interest [49].

It is quite interesting that, despite the reports concerning Schiff bases of 3-quinazolinone derivatives and their metal complexes [11–14], there are no reports about metal complexes among hydrazines and their hydrazone derivatives located at position 2 of quinazolinone. This specific location resembles the important biological molecule guanine. Within this context, we have designed, synthesized and characterized a novel pyridine derivative of 2-quinazolinone hydrazone ligand (HL). With this guanine-based bioinspired ligand (L) we have targeted a series of Cu(II), Ni(II) and Zn(II). All coordination compounds have been synthesized and characterized by diverse spectroscopic techniques and single-crystal X-ray crystallography. The potential biological relevance of the novel compounds (HL and its complexes) has been evaluated in regard to: (I) their binding affinity towards calf-thymus (CT) DNA studied by a) UV–vis spectroscopy, b) cyclic voltammetry, c) viscosity measurements and d) fluorescence emission spectroscopy for ethidium bromide (EB) competitive studies; (II) their ability to induce cleavage to supercoiled circular pBR322 plasmid DNA in the absence or presence of irradiation with UVA, UVB and visible light; (III) their binding to serums albumins, especially bovine (BSA) and human (HSA) serum albumin, investigated by fluorescence emission spectroscopy, and the location of binding site, and (IV) their scavenging activity towards free radicals 1,1-diphenyl-picrylhydrazyl (DPPH) and 2,2′-azinobis-(3-ethylbenzothiazoline-6-sulfonic acid) (ABTS).

2. Experimental

2.1. Materials and instrumentation

All necessary chemicals and solvents were reagent grade and were used as purchased from commercial sources, i.e. 2,4-dichloroquinazoline and ibuprofen were purchased from Fluorochem; hydrazine hydrate ($H_2NNH_2{\cdot}H_2O$) and $ZnCl_2$ from Alfa Aesar; 2-pyridine-carboxaldehyde, warfarin, 6-hydroxy-2,5,7,8-tetramethylchromane-2-carboxylic acid (trolox) and ABTS from J&K; $Cu(NO_3)_2{\cdot}2.5H_2O$ and $Ni(NO_3)_2{\cdot}6H_2O$ from Merck; BSA, HSA, CT DNA, EB, DPPH, potassium persulfate, nordihydroguaiaretic acid (NDGA), butylated hydroxytoluene (BHT) from Sigma-Aldrich Co; Tris base, boric acid, EDTA disodium salt dehydrate, Loading buffer from PanReac Applichem; supercoiled circular pBR322 plasmid DNA from New England Bioline; and all solvents from Chemlab.

The CT DNA stock solution was prepared by dissolving CT DNA to a buffer solution (containing 150 mM NaCl and 15 mM trisodium citrate at pH 7.0) which was followed by 3-day stirring and was kept at 4 °C for no longer than two weeks. The concentration of this DNA solution was determined by the UV absorbance of a 1:20 diluted solution at 260 nm using $\varepsilon = 6600\ M^{-1}\ cm^{-1}$ [50]. The ratio of UV absorbance at 260 and 280 nm (A_{260}/A_{280}) of the stock DNA solution was higher than 1.85, which may imply the protein non-contamination of DNA [51].

Infrared (IR) spectra were recorded in the range 400–4000 cm^{-1}on a Nicolet FT-IR 6700 spectrometer with samples prepared as KBr pellets. UV–vis spectra were recorded as nujol mulls and in solution at concentrations in the range 10^{-5}–10^{-3} M on a Hitachi U-2001 dual beam spectrophotometer. C, H and N elemental analysis was performed on a Perkin-Elmer 240B elemental analyzer. ^1H NMR spectra and $^1H-^1H$ NMR correlation (COSY) spectra were recorded on an Agilent DD2 500 MHz spectrometer in DMSO-d_6 as solvent. The numbering of the H atoms used for the NMR spectra of HL and complex **4** is given in Fig. S5. The molar conductivity measurements of a solution of the complexes in DMSO (1 mM) were performed with a Crison Basic 30 conductometer. Room temperature magnetic measurements were carried out by the Faraday method using mercury tetrathiocyanatocobaltate(II) as a calibrant. The fluorescence spectra were recorded in solution on a Hitachi F-7000 fluorescence spectrophotometer. The viscosity experiments were performed with an ALPHA L Fungilab rotational viscometer equipped with an 18-mL LCP spindle. The High Resolution Mass Spectra measured with a Q-TOF (Time of Flight Mass Spectrometry) Bruker Maxis Impact with ESI source and U-HPLC Thermo Dionex Ultimate 3000 pump and autosampler. N_2 was used as collision gas and electrospray ionization (ESI) was used for the MS experiments. The data acquisition was carried out with Data analysis from Bruker Daltonics (version 4.1).

Cyclic voltammetry studies were performed on an Eco chemie Autolab Electrochemical analyzer. Cyclic voltammetry experiments were carried out in a 30-mL three-electrode electrolytic cell. The working electrode was platinum disk, a separate Pt single-sheet electrode was used as the counter electrode and a Ag/AgCl electrode saturated with KCl was used as the reference electrode. The cyclic voltammograms of the complexes were recorded in 0.4 mM 1/2 DMSO/buffer solutions at $v = 100\ mV\ s^{-1}$ where buffer solution was the supporting electrolyte. Oxygen was removed by purging the solutions with pure nitrogen which had been previously saturated with solvent vapors. All electrochemical measurements were performed at 25.0 ± 0.2 °C.

2.2. Synthesis of HL

The synthesis of HL took place in two stages. In the first stage, 2,4-dichloroquinazoline (8 mmol, 1592 mg) (I in Scheme 1) was dissolved in THF (12 mL) and the mixture was stirred for 1 h after the addition of 36 mL NaOH. Then CH_3COOH was added dropwise until the pH became

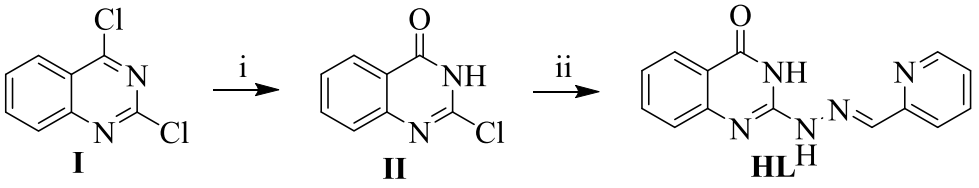

Scheme 1. Synthesis of the ligand HL. Reaction conditions: i) NaOH, THF, CH_3COOH. 1 h, 83% yield; ii) $NH_2NH_2{\cdot}H_2O$, 2-pyr-CHO, EtOH, 100 °C, 15 min, MW, 88% yield.

≈5. The solution was filtered off, and the resultant 2-chloroquinazolin-4(3H)-one (II in Scheme 1) was washed with water and dried. Yield: 83% (1200 mg) [52].

In the second stage, 2-chloroquinazolin-4(3H)-one (500 mg) was dissolved in EtOH (2 mL), and subsequently hydrazine hydrate (178.50 μL) as well as 2-pyridine-carboxaldehyde (316.05 μL) were added (molar ratio for 2-chloroquinazolin-4(3H)-one: hydrazine hydrate: 2-pyridine-carboxaldehyde 1:1.3:1.2). The mixture was heated in a microwave oven at 100 °C for 15 min. A yellow solid (HL) was formed, which was filtered off, washed with EtOH, dried in vacuum and recrystallized by EtOH. Yield 88% (646 mg). *Anal.* calcd. for $C_{14}H_{11}N_5O_1$ (MW = 265.10): C 63.39, 4.18, N 26.40; found C 63.55, 4.27, N 26.17%; IR (KBr disk), ν_{max}/cm^{-1}: ν(N—H): 3421 (medium (m)), 3148 (m); ν(C=O): 1678 (very strong (vs)); ν(C=C): 1608 (vs); ν(C—NH)$_{arom}$: 1562 (strong (s)); ρ(C—H)$_{quin}$: 776 (m); ρ(C—H)$_{pyr}$: 686 (m). UV–vis in DMSO, λ/nm (ε/M^{-1} cm^{-1}): 402 (5900), 330 (10500), 302 (sh) (7500). ^{1}H NMR (DMSO-d_6), δ (ppm) (the numbering of the H atoms is shown in Fig. S5): 8.80 (d, J = 4.5 Hz, 1H, H$^{6'}$), 8.50 (brs, 1H, H$^{4'}$), 8.35 (brs, 2H, H$^{3'}$ and H^{a}), 7.85 (d, J = 7.4 Hz, 1H, H^5), 7.86 (brs, 1H, H$^{5'}$), 7.71 (t, J = 7.1 Hz, 1H, H^7), 7.26 (t, J = 7.1 Hz, 1H, H^6). ESI-MS: Calculated for $C_{14}H_{11}N_5O$: M = 265; Found: [M + H]$^+$ = 266, [M - H]$^-$ = 264. The compound is soluble in MeOH, DMF, $CHCl_3$ and DMSO.

2.3. Synthesis of the complexes

2.3.1. [CuL(H$_2$O)$_2$](NO$_3$)·H$_2$O, 1·H$_2$O

A methanolic solution (10 mL) containing HL (0.1 mmol, 26.5 mg) was added, after 30-min stirring, dropwise to a methanolic solution (5 mL) of $Cu(NO_3)_2{\cdot}2.5H_2O$ (0.1 mmol, 23.2 mg). The reaction solution was stirred for additional 30 min and was left to slowly evaporate. After ten days, green crystalline product of [Cu(L)(H$_2$O)$_2$](NO$_3$), **1** (25 mg, 70%) suitable for X-ray structure determination was collected. HRMS (ESI) in MeOH, found (calcd) (*m/z*): 345.0266 (345.0282 for [Cu(L)(H$_2$O)]$^+$); 327.0181 (327.0176 for [Cu(L)]$^+$). *Anal.* calcd. For$C_{14}H_{16}CuN_6O_7$ (MW = 443.86): C 37.88, 3.63, N 18.93; found: C 38.05, H 3.58, N 18.67%. IR (KBr disk), ν_{max}/cm^{-1}: ν(N—H): 3422 (m), 3169 (m); ν(C=O): 1630 (vs); ν(C=C): 1606 (vs); ν(C-NH)$_{arom}$: 1567 (s); ρ(C—H)$_{quin}$: 774 (m); ρ(C—H)$_{pyr}$: 691 (m). UV–vis as nujol mull, λ/nm: 625, 405 (sh); UV–vis in DMSO, λ/nm (ε/M^{-1} cm^{-1}): 620 (100); 400 (18500), 265 (24000). μ$_{eff}$ at room temperature = 1.81 BM. The complex is soluble DMSO. Λ_M = 75 S·cm^2·mol^{-1}, 1 mM in DMSO.

2.3.2. [CuL$_2$], 2

A methanolic solution (20 mL) of HL (0.2 mmol, 53 mg) was added, after 30-min stirring and heating, dropwise to a methanolic solution (10 mL) of $Cu(NO_3)_2{\cdot}2.5H_2O$ (0.1 mmol, 24.1 mg). The reaction solution was stirred for additional 30 min at room temperature and was left to evaporate. The deep-green solid product (35 mg, 60%) that was formed immediately, filtered and dried in air. HRMS (ESI) in MeOH, found (calcd) (*m/z*): 592.1145 (593.1139 for [Cu(L)$_2$ + H]$^+$); 345.0271 (345.0282 for [Cu(L)(H$_2$O)]$^+$). Anal. calcd. For $C_{28}H_{20}N_{10}O_2Cu$ (MW = 592.08): C 56.80, 3.40, N 23.66; found: C 56.55, H 3.49, N 23.45%. IR (KBr disk), ν_{max}/cm^{-1}: ν(N—H): 3432 (m), 3160 (m); ν(C=O): 1676 (vs); ν(C=C): 1607 (vs); ν(C-NH)$_{arom}$: 1566 (s); ρ(C—H)$_{quin}$: 757 (m); ρ(C—H)$_{pyr}$: 683 (m). UV–vis as nujol mull, λ/nm: 685, 410 (sh); UV–vis in DMSO, λ/nm (ε/M^{-1} cm^{-1}): 675 (115), 415 (17000), 300 (12200), 265 (13300). μ$_{eff}$ at room temperature = 1.85 BM. The complex is soluble in DMSO. Λ_M = 10 S·cm^2·mol^{-1}, 1 mM in DMSO.

2.3.3. [NiL$_2$], 3

Complex **3** was prepared in a similar way with complex **2** with the use of $Ni(NO_3)_2{\cdot}6H_2O$ (29 mg, 0.1 mmol) in the place of $Cu(NO_3)_2{\cdot}2.5H_2O$. Orange microcrystalline product of **3** (32 mg, 55%) was collected after two weeks. HRMS (ESI) in MeOH, found (calcd) (*m/z*): 587.1198 (587.1197 for [Ni(L)$_2$ + H]$^+$). *Anal.* calcd. For$C_{28}H_{20}N_{10}O_2Ni$ (MW = 587.24): C 57.27, 3.43, N 23.85; found: C 57.46, 3.56, N 23.61%. IR (KBr disk), ν_{max}/cm^{-1}: ν(N—H): 3437 (m), 3217 (m); ν(C=O): 1663 (vs); ν(C=C): 1627 (vs); ν(C—NH)$_{arom}$: 1578 (s); ρ(C—H)$_{quin}$: 752 (m); ρ(C—H)$_{pyr}$: 689 (m). UV–vis as nujol mull, λ/nm: 805 (sh), 615, 435 (sh); UV–vis in DMSO, λ/nm (ε/M^{-1} cm^{-1}): 830 (20), 605 (shoulder (sh)) (35), 450 (sh) (2500), 415(17500), 300 (13000). μ$_{eff}$ at room temperature = 3.02 BM. The complex is soluble in DMSO. Λ_M = 12 S·cm^2·mol^{-1}, 1 mM in DMSO.

2.3.4. [ZnL$_2$], 4

Complex **4** was prepared similarly to complex **2**. $ZnCl_2$ (0.1 mmol, 14 mg) was used instead of $Cu(NO_3)_2{\cdot}2.5_2O$. Light-yellow microcrystalline product of **4** (30 mg, 50%) was collected after ten days. HRMS (ESI) in MeOH, found (calcd) (*m/z*): 593.1134 (593.1135 for [Zn(L)$_2$ + H]$^+$). Anal. calcd. for $C_{28}H_{20}N_{10}O_2Zn$ (MW = 593.91): C 56.63, 3.39, N 23.59; found: C 56.45, 3.28, N 23.37%. IR (KBr disk), ν_{max}/cm^{-1}: ν(N—H): 3454 (m), 3211 (m); ν(C=O): 1692 (s); ν(C=C): 1619 (vs); ν(C-NH)$_{arom}$: 1552 (s); ρ(C—H)$_{quin}$: 760 (m); ρ(C—H)$_{pyr}$: 687 (m). UV–vis in DMSO, λ/nm (ε/M^{-1} cm^{-1}): 405(sh) (1300), 340 (14500), 267 (12500). ^{1}H NMR (DMSO-d_6), δ (ppm) (the numbering of the H atoms is shown in Fig. S5): 8.63 (s, 2H, H$^{6'}$), 8.48 (brs, 2H, H$^{3'}$), 8.17 (s, 2H, H^{a}), 8.04 (brs, 2H, H$^{4'}$), 7.95 (d, 2H, H^5), 7.65 (s, 2H, H^7), 7.51 (s, 2H, H$^{5'}$), 7.37 (s, 2H, H^8), 7.20 (s, 2H, H^6). The complex is soluble in DMSO. Λ_M = 8 S·cm^2·mol^{-1}, 1 mM in DMSO.

2.4. X-ray structure determination

Single-crystals of complex **1** suitable for X-ray diffraction were mounted on a Bruker Kappa APEX 2 diffractometer, equipped with a triumph monochromator using MoKa radiation at ambient temperature. Cell dimensions refinement was accomplished using at least 100 high θ reflections. The crystal presented no decay during the data collection. The frames collected (running φ and ω scans) were integrated with the Bruker SAINT Software package [53], using a narrow-frame algorithm. Data were corrected using the SADABS program [54]. The structure was solved by the SUPERFLIP package [55]. Crystals program package version 14.61 [56] was used for the refinement and all the rest subsequent calculations through full-matrix least-squares on F^2. All non-hydrogen non-disordered atoms have been refined anisotropically. Hydrogen atoms bonded were found at their expected positions and refined using proper riding constraints to the pivot atoms. CAMERON program has been used to produce molecular illustrations [57]. Crystallographic and experimental details are summarized in Table S1.

2.5. Interaction of the compounds with DNA

2.5.1. Binding studies with CT DNA

In order to study the interaction of complexes with DNA, the compounds were initially dissolved in DMSO (1 mM). Mixing of such solutions with the aqueous buffer solutions of DNA or BSA used in the studies never exceeded 5% DMSO (*v/v*) in the final solution, which was needed due to low aqueous solubility of most compounds. In all experiments, the effect of DMSO on the data was taken into consideration and the appropriate corrections were performed. The interaction of the compounds with CT DNA was studied by UV–vis spectroscopy, cyclic voltammetry and viscosity measurements and *via* competitive studies with EB by fluorescence emission spectroscopy.

2.5.1.1. UV–vis spectroscopy. UV–vis spectroscopy was used to study the interaction of the compounds with CT DNA in order to estimate their possible binding mode to CT DNA and calculate the corresponding binding constants (K_b). The UV spectra of CT DNA in the presence of each compound were recorded for a constant CT DNA concentration (1.4–1.6 × 10^{-4} M) at diverse [compound]/[CT DNA] mixing ratios (*r*). The UV–vis spectra of the compounds recorded for a standard concentration (20–30 μM) in the absence or presence of increasing concentration of CT DNA for diverse r values were used to calculate the values of the constant K_b (in M^{-1}) by the Wolfe-Shimer equation (Eq. S1) [58] and the plots [DNA]/(ε_A-ε_f) *versus* [DNA]. Control experiments with DMSO were performed and no changes in the spectra of CT DNA were observed.

2.5.1.2. DNA-viscosity measurements. The viscosity of DNA solution in buffer solution (150 mM NaCl and 15 mM trisodium citrate at pH 7.0) was measured upon increasing amounts of the compounds (up to the value of r = 0.35). All measurements were performed at room temperature and the obtained data are presented as $(\eta/\eta_0)^{1/3}$ *versus r*, where η is the viscosity of DNA in the presence of the compound and η_0 is the viscosity of DNA alone in buffer solution.

2.5.1.3. Cyclic voltammetry. The interaction of complexes **1–3** with CT DNA was also investigated *via* monitoring the changes observed in the cyclic voltammogram of a 0.40 mM 1:2 DMSO:buffer solution of the complex upon addition of DNA solution at diverse *r* values. The buffer was also used as the supporting electrolyte and the cyclic voltammograms were recorded at ν = 100 mV s^{-1}. The ratio of the DNA-binding constants for the reduced (K_r) and oxidized forms (K_{ox}) of the complexes (K_r/K_{ox}) was calculated according to Eq. S2 [59].

2.5.1.4. EB-competitive studies. The competitive studies of the compounds with EB for the DNA-intercalating sites (by displacing it from its DNA-EB complex) were investigated with fluorescence emission spectroscopy. The CT DNA-EB complex was prepared by pre-treating 20 μM EB and 30 μM CT DNA in buffer (150 mM NaCl and 15 mM trisodium citrate at pH 7.0). The possible replacement of EB by the compounds and, thus, the intercalating effect was studied by the stepwise addition of a certain amount of a compound's solution into a solution of the DNA-EB conjugate. The effect of the addition of each complex to the DNA-EB complex solution was obtained by recording the variation of fluorescence emission spectra with excitation wavelength at 540 nm [60]. The complexes do not show any appreciable fluorescence emission bands at room temperature in solution or in the presence of CT DNA or EB under the same experimental conditions (λ_{ex} = 540 nm); therefore, the observed quenching of the EB-DNA solution may be attributed to the displacement of EB from its EB-DNA conjugate. The Stern–Volmer constants (K_{SV}, in M^{-1}) were calculated according by the linear Stern–Volmer equation (Eq. S3) [61] and the respective plots Io/I *versus* [Q]. Taking τ_o = 23 ns as the fluorescence lifetime of the EB-DNA conjugate [62], the quenching constants (k_q, in M^{-1} s^{-1}) of the complexes were calculated according to Eq. S4.

2.5.2. DNA photo-cleavage experiments

The reaction mixtures (20 μL) containing supercoiled circular pBR322 plasmid DNA (New England Bioline), compounds, and Tris buffer (25 μM, pH 6.8) in PCR plastic tubes were incubated for 30 min at 37 °C, centrifuged (Nippon Genetics Europe GmbH FastGene Mini Centrifuge), and then irradiated, under aerobic conditions at room temperature, with UVB light/9W/01/2P narrow-band (312 nm, 2 × 9 W) for 30 min at 15-cm distance, or UVA light 9 W/10/2P lamps (2 × 9 W, Philips, Pila, Poland) at 365 nm, 10-cm distance for 2 h and or visible light with 9 W/71/G23 lamps (2 × 9 W, OSRAM 71 COLOR), 10-cm distance for 2 h.

After addition of the gel-loading buffer (PanReac AppliChem), the reaction mixtures were loaded on a 1% agarose (Canvax) gel with EB staining. The electrophoresis tank (Mupid-One Submarine Electrophoresis System) was attached to a power supply at a constant current (70 V for 1 h). The gel was visualized by Mupid Led Illuminator (Nippon Genetics Europe GmbH) and photographed with a DSLR camera Nikon AF-S 18–105 mm f/3.5–5.6 VR. Quantification of DNA-cleaving activities was performed by integration of the optical density as a function of the band area using the program "Image J" version 1.50.I available at the site *http://rsb.info.nih.gov/ij/download.html* and the single-strand (ss%) as well as double-strand (ds%) damage was calculated, using a correction factor of 1.43 [63]. The ss% and ds% damage was calculated according to the following Eqs. (1) and (2).

$$ss\% = \frac{FormII}{(FormI+FormII+FormIII)} \times 100 \quad (1)$$

$$ds\% = \frac{FormIII}{(FormI+FormII+FormIII)} \times 100 \quad (2)$$

where as Form II we consider Form II of each series minus Form II of the irradiated control DNA. As Form I, we consider Form I of each series.

2.6. Albumin assays

2.6.1. Albumin-binding studies

The albumin-binding study was performed by tryptophan fluorescence quenching experiments using BSA (3 μM) or HSA (3 μM) in buffer (containing 15 mM trisodium citrate and 150 mM NaCl at pH 7.0). The fluorescence emission spectra were recorded with an excitation wavelength of 295 nm. The quenching of the emission intensity of tryptophan residues of BSA at 343 nm or HSA at 340 nm was monitored using HL or its complexes **1–4** as quenchers with gradually increasing concentration [60]. Except to this, the fluorescence emission spectra of the compounds were also recorded with λ_{ex} = 295 nm and an emission band appeared at λ_{max} = 440–445 nm for complexes **2–4**; so, the SA-fluorescence emission spectra were corrected by subtracting the spectra of the compounds. The influence of the inner-filter effect on the measurements was evaluated by Eq. S5 [64]. The Stern–Volmer and Scatchard equations (Eqs. S3, S4 and S6) [65] and graphs were used in order to calculate the Stern-Volmer constant K_{SV} (in M^{-1}), the quenching constant k_q (in M^{-1} s^{-1}), the SA-binding constant (K, in M^{-1}) and the number of binding sites per albumin n.

2.6.2. Competitive SA-fluorescence studies with warfarin and ibuprofen

The competitive studies with warfarin or ibuprofen (site probes) were performed by tryptophan fluorescence quenching experiments using a fixed concentration of the serum albumin (SA) and site probes (3 μM) in buffer (containing 15 mM trisodium citrate and 150 mM NaCl at pH 7.0). The fluorescence emission spectra were recorded in the presence of increasing amounts of HL or its complexes **1–4** as quenchers and in the range 300 to 500 nm with an excitation wavelength of 295 nm. The Scatchard equation (Eq. S6) [65] and plots were applied on the corrected SA-fluorescence emission spectra in order to determine

the SA-binding constant (K, in M^{-1}) of the compounds in the presence of warfarin or ibuprofen.

2.7. Antioxidant biological assay

The antioxidant activity of the compounds was evaluated *via* their ability to scavenge *in vitro* free radicals such as DPPH and ABTS. All the experiments were carried out at least in triplicate and the standard deviation of absorbance was less than 10% of the mean.

2.7.1. Determination of the reducing activity of the stable radical DPPH

To an ethanolic solution of DPPH (0.1 mM) an equal volume solution of the compounds (0.1 mM) in ethanol was added. Absolute ethanol was also used as control solution. The absorbance at 517 nm was recorded at room temperature after 20 and 60 min, in order to examine the possible existence of a potential time-dependence of the DPPH radical scavenging activity [66]. The DPPH-scavenging activity of the complexes was expressed as the percentage reduction of the absorbance values of the initial DPPH solution (DPPH%). NDGA and BHT were used as reference compounds.

2.7.2. Assay of radical cation ABTS-scavenging activity

Initially, a water solution of ABTS was prepared (2 mM). ABTS radical cation ($ABTS^{+\cdot}$) was produced by the reaction of ABTS stock solution with potassium persulfate (0.17 mM) and the mixture was stored in the dark at room temperature for 12–16 h before its use. The ABTS was oxidized incompletely because the stoichiometric reaction ratio of ABTS and potassium persulfate is 1:0.5. The absorbance became maximal and stable only after more than 6 h of reaction although the oxidation of the ABTS started immediately. The radical was stable in this form for more than 2 days when allowed to stand in the dark at room temperature. Afterwards, the $ABTS^{+\cdot}$ solution was diluted in ethanol to an absorbance of 0.70 at 734 nm and 10 μL of diluted compounds or standards (0.1 mM) in DMSO were added. The absorbance was recorded out exactly 1 min after initial mixing [66]. The ABTS radical scavenging activity of the complexes was expressed as the percentage inhibition of the absorbance of the initial ABTS solution (ABTS%). Trolox was used as an appropriate standard.

3. Results and discussion

3.1. Synthesis and characterization of HL

HL (Fig. 1(C)) was designed in a way to fulfill various criteria. Initially, such a compound resembles partially with guanine. Guanine (Fig. 1(A)), as a DNA-base exhibits three sites for hydrogen bonding. The structure of both guanine and 2-amino-(or 2-hydrazinyl)quinazolinone incorporates the guanidine pharmacophore (Fig. 1(B)). Addition of *o*-pyridine moiety in the form of a hydrazone provides additional positions for hydrogen bond donors and acceptors. To the best of our knowledge, no complexation with any metal appeared in the literature so far. The final scaffold provides an interesting structure, able to challenge a metal to "recognize" a preferred site for reaction.

In order to target the desired structure, we have transformed commercially available 2,4-dichloro-quinazoline (**I**) into 2-Cl-quinazolinone precursor (**II**) using NaOH solution [52] (Scheme 1). Continuously, compound **II** reacted under microwave irradiation with hydrazine hydrate and *o*-pyridine carboxaldehyde to give the desired ligand HL in very good yield. Spectroscopic data and X-ray analysis of the complex correspond to the proposed structure.

3.2. Synthesis and characterization of the complexes

The complexes were prepared *via* the aerobic reaction of HL with a methanolic solution of the corresponding salt of the metal (Cu $(NO_3)_2{\cdot}2.5H_2O$, $Ni(NO_3)_2{\cdot}6H_2O$ or $ZnCl_2$) in a 1:1 or 1:2 metal:HL ratio. Complexes **1–4** have been characterized by HRMS, IR, ^1H NMR and UV–vis spectroscopies, molecular conductance and room-temperature magnetic measurements and single-crystal X-ray crystallography.

For the 1:1 metal:HL ratio, only the copper complex **1** was isolated and characterized; the X-ray crystal structure revealed a 1:1 Cu:L composition (as also shown by HRMS data, Fig. S1). For the 1:2 metal:HL ratio, microcrystalline products of all three tested metal (Cu (**2**), Ni (**3**) and Zn (**4**)) were isolated. According to the data collected, the complexes have a 1:2 metal:L composition (in the HRMS, fragments very close to the expected molecular ions were observed, Figs. S2–S4). The compounds are air-stable, soluble mainly in DMSO and insoluble in most common organic solvents and water.

The molar conductivity values of the complexes in 1 mM DMSO solution (Λ_M = 75 $S{\cdot}cm^2{\cdot}mol^{-1}$ for **1** and 8–12 $S{\cdot}cm^2{\cdot}mol^{-1}$ for **2–4**) indicate an electrolytic (1:1) nature of complex **1** and the non-electrolytic nature of complexes **2–4** (since in the case of a 1:1 electrolyte, the Λ_M value of a 1 mM DMSO solution should be higher than 70 $S{\cdot}cm^2{\cdot}mol^{-1}$ [67]) and may show the integrity of the complexes in solution.

The IR spectra of the compounds are rather complicated due to the presence of similar different characteristic groups, such as the aromatic quinazolinone and the pyridine rings [68]. The assignment of the most characteristic IR peaks was accomplished *via* comparisons with literature [69,70]. In the IR spectra of the compounds, all characteristic bands of the deprotonated ligand (L) were determined. Complexes **2–4** have similar IR spectral patterns suggesting a similar structure, while the IR spectrum of complex **1** bears some differences, such as the position of the ν(C=O) (1630 cm^{-1}) and the $\rho(C{-}H)_{quinazoline}$ (774 cm^{-1}) in contrast with **2–4** which are located at 1663–1692 cm^{-1} and 750–760 cm^{-1}, respectively.

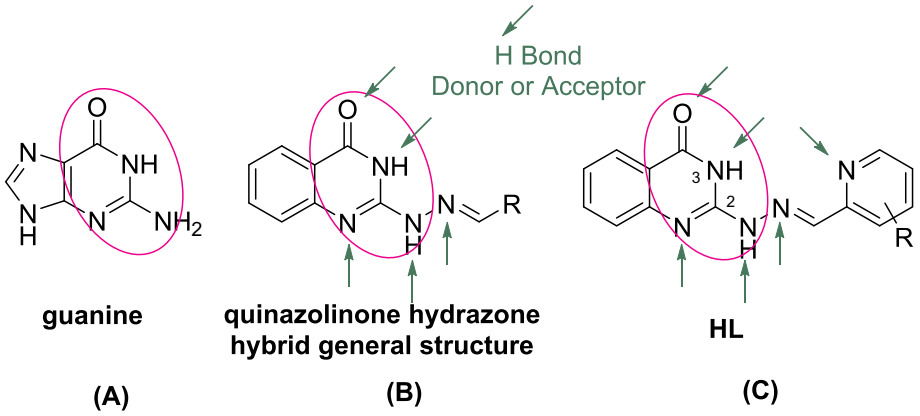

Fig. 1. The syntax formula of (A) guanine, (B) quinazolinone hydrazone and (C) HL (for R = H).

The ^{1}H NMR spectra and the ^{1}H–^{1}H NMR correlation (COSY) spectra of HL and complex **4** were recorded in DMSO-d_6 solution so that their behavior in solution is investigated (the numbering of the H atoms is shown in Fig. S5). It is quite interesting that in the spectra of HL (Figs. S6 and S7), the signal expected for H^8 of quinazolinone ring is obscured, while the signals attributed to imine H (H^a) and $H^{3'}$ of the pyridine ring are not separated giving a broad peak. In the NMR spectra of complex **4** (Figs. S8 and S9), nine signals attributed to the hydrogen atoms of ligand L were observed and some of them were slightly shifted as expected upon binding to Zn ion. In particular, the signal for H^8 of quinazolinone ring can be located at 7.37 ppm, while (H^a) and $H^{3'}$ show separate signals at 8.17 ppm and 8.48 ppm, respectively. No other signals which might be assigned to dissociated ligands were located showing that complex **4** keeps its integrity in solution; this is in good agreement with the molar conductance measurements. The ^{1}H NMR spectrum of the complex was also recorded for diverse time intervals up to 48 h (Fig. S10); the absence of any changes in the spectrum may reveal that complex **4** remains stable in solution during time.

The UV–vis spectra of the complexes were recorded in DMSO solution and as nujol mull. The UV–vis spectra of complexes **1–3** in solid state (nujol) bear similar patterns with those recorded in DMSO solution, therefore the stability of the complexes in solution may be suggested. In the visible region of the spectra, bands assigned to d-d transitions were observed. For the Cu(II) complexes the differences in the location of d-d characteristic band may suggest different geometry around copper; in **1**, the d-d band was located at 620 nm (ε = 100 M^{-1} cm^{-1}) and may rather suggest a square pyramidal geometry resulting from five-coordination, while for **2** the band was observed at 675 nm (ε = 115 M^{-1} cm^{-1}) showing a distorted octahedral geometry around copper and subsequently six-coordination [71,72]. For the Ni(II) complex **3**, three characteristic bands were observed; band I attributed to a $^3A_{2g}$ ➔ $^3T_{2g}$ transition was found at 830 nm (ε = 20 M^{-1} cm^{-1}), band II assigned to a $^3A_{2g}$ ➔ $^3T_{1g}$ transition was observed at 605 nm (ε = 35 M^{-1} cm^{-1}) and band III for a $^3A_{2g}$ ➔ $^3T_{1g}$(P) transition appeared as a shoulder at 450 nm which was overlapped by the nearby strong band at 415 nm. The existence and the location of these three bands assigned to d–d transitions are characteristic for distorted octahedral Ni^{2+} complexes [31]. In the UV region of the electronic spectra of the complexes in DMSO, characteristic band appeared in similar regions with HL, i.e. 400–415 nm, and 300–340 nm which could be assigned to intra-ligand transitions.

The magnetic measurements for complexes **1–3** were carried out at room temperature. The results showed that the μ_{eff} values for the compounds (1.81–1.85 for **1** and **2**, and 3.02 BM for **3**) are slightly higher than the expected spin-only value (=1.73 BM and 2.83 BM, respectively) and are typical for mononuclear Cu(II) and Ni(II) complexes with d^9 and d^8 (high-spin) configuration, respectively [31,40,41,71].

3.3. Structure of the complexes

For compound **1**, single-crystals suitable for X-ray crystallography have been obtained. Therefore, the crystal structure of compound **1** was determined by X-ray crystallography. Complexes **2–4** were obtained as microcrystalline products and their structures are proposed based on all experimental data and in comparison with compound **1**.

3.3.1. X-ray crystal structure of 1

A diagram of the crystal structure of compound $[Cu(L)(H_2O)_2](NO_3)\cdot H_2O$, **1**, is shown in Fig. 2, and selected bond distances and angles are cited in Table 1. The molecule consists of a cationic mononuclear complex $[Cu(L)(H_2O)_2]^+$ which is neutralized by a nitrate anion, while the solvate water molecule is H-bonded to the cationic complex.

In the cationic complex $[Cu(L)(H_2O)_2]^+$, the quinazolinone ligand is deprotonated and is bound tridentately to copper atom *via* three nitrogen atoms, i.e. the pyridine nitrogen (N1), the hydrazine nitrogen (N2) and the quinazolinone nitrogen (N4), forming two five-membered chelate rings. The coordination sphere of copper is completed by two oxygen atoms O(2) and O(3) of the coordinated aqua ligands. The copper atom is five-coordinate and its coordination sphere may be described as distorted square pyramidal geometry, as suggested by the values of the trigonality index τ = (165.47° − 159.61°) / 60° = 0.098 [τ = (φ_1 − φ_2) / 60°, where φ_1 and φ_2 are the largest angles in the coordination sphere; τ = 0 for a perfect square pyramid and τ = 1 for a perfect trigonal bipyramid] [73] and the tetragonality T^5 = 0.897 (which is based on the changes in bond lengths [72]) showing slight distortion from the regular square-based pyramidal geometry. The three nitrogen atoms N(1), N(2) and N(4) of the ligand L and the oxygen atom O(3) form the basal plane of the pyramid and O(2) occupies the apical position. The copper atom is displaced by 0.194 Å from the mean basal plane towards the aqua oxygen O(2).

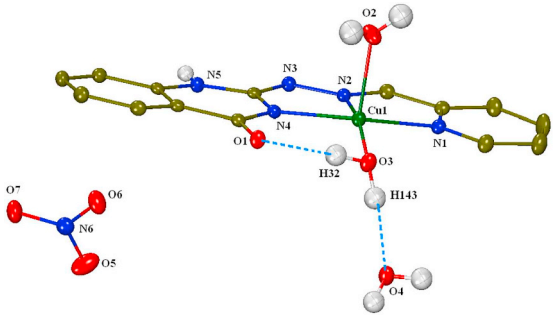

Fig. 2. Molecular structure of complex **1**. The hydrogen atoms are omitted for clarity. Hydrogen bonds are in depicted with blue dotted lines.

Table 1
Selected bonds distances (Å) and angles (°) for complex **1**.

Bond	Distance (Å)	Bond	Distance (Å)
Cu(1)-N(1)	1.9994(18)	Cu(1)-N(4)	1.9758(17)
Cu(1)-N(2)	1.9432(16)	Cu(1)-O(3)	1.9865(15)
Cu(1)-O(2)	2.2043(17)		
N(2)-N(3)	1.359(2)	N(3)-C(7)	1.328(3)
N(2)-C(6)	1.278(3)	N(4)-C(7)	1.366(2)

Bonds	Angle (°)	Bonds	Angle (°)
N(1)-Cu(1)-N(2)	81.20(7)	N(1)-Cu(1)-O(2)	96.35(7)
N(1)-Cu(1)-N(4)	159.61(7)	N(1)-Cu(1)-O(3)	99.48(7)
N(2)-Cu(1)-N(4)	79.23(7)	N(2)-Cu(1)-O(2)	101.68(7)
N(2)-Cu(1)-O(3)	165.47(7)	N(4)-Cu(1)-O(2)	93.16(7)
N(4)-Cu(1)-O(3)	98.03(7)	O(2)-Cu(1)-O(3)	92.69(8)

The structure of the complex is stabilized by the presence of intra- and intermolecular hydrogen bonds. An intramolecular H-bond is formed between the quinazolinone O(1) and H(32) of one coordinated H_2O ligand (Table S2) being in the base of square pyramid. The second H(143) of this coordinated aqua ligand forms a H-bond with the oxygen atom O(4) of the solvate H_2O molecule. The solvate O(4) is also H-bonded with N(5) of a neighboring molecule. The nitrate anions are hydrogen-bonded *via* O(6) with O(4) of the solvate water molecule and through O(6) and O(7) with the apical O(2) of the second coordinated aqua ligand of two neighboring molecules. The presence of all these intermolecular H-bonds results in the formation of an extended H-bond network.

3.3.2. Proposed structures for complexes 2–4

Our continuous efforts to crystallize compounds **2–4** did not yield any single-crystals suitable for X-ray crystallography. Therefore, the characterization of these compounds is based on the data collected by IR, HRMS, ^{1}H NMR and UV–vis spectroscopies and magnetic and molecular conductance measurements.

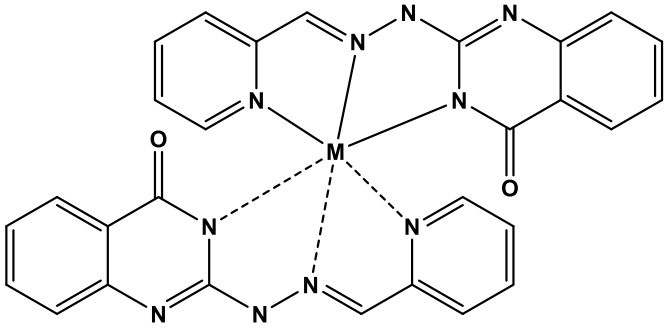

Fig. 3. Proposed structures for complexes **2–4** (M = Cu for **2**, Ni for **3** and Zn for **4**).

Based on the data derived from MS, the complexes are isostructural bearing the molecular formula $[ML_2]$, where the quinazolinone ligand is deprotonated. The similarity of the IR spectra of complexes **1–4** suggests that each ligand L is coordinated to the metal atom in complexes **2–4** in the same way as that described for the structure of complex **1**, i.e. the L ligands are bound to M tridentately *via* the pyridine, the hydrazine and the quinazolinone nitrogen atoms. In addition, the molecular conductance measurements reveal their non-electrolytic character of complexes **2–4**. For complexes **2** and **3**, the magnetic data may indicate the mononuclear nature of the complexes and the electronic spectra are typical for octahedral environment around the metals implying their six-coordination. The proposed structures of complexes **2–4** are depicted in Fig. 3.

3.4. Interaction of the compounds with CT DNA

The interaction of HL and complexes **1–4** with CT DNA was investigated by UV–vis spectroscopy, viscosity titrations, cyclic voltammetry and *via* competitive studies with EB which were monitored by fluorescence emission spectroscopy.

3.4.1. CT DNA-binding study with UV–vis spectroscopy

UV–vis spectroscopy is a technique commonly used as first means to evaluate the interaction between DNA and the complexes, and so it may provide information about the mode of interaction of metal complexes with CT DNA and the strength of this interaction [45]. The UV spectra of a CT DNA solution were recorded in the presence of HL and its complexes **1–4** at increasing amounts (for different r = [compound]/[CT DNA] values) as well as the UV spectra of the compounds in the presence of CT DNA at increasing amounts. The existence of any interaction will perturb the band of CT DNA at 258–260 nm or the intraligand transition bands of the compounds during the titrations providing initial information of such interaction [74].

The UV–vis spectra of a CT DNA buffer solution upon addition of increasing concentration of complex **3** are shown representatively in Fig. 4(A). The slight hypochromism that the DNA UV-band at λ_{max} = 258 nm presents upon the addition of the complexes may indicate the existence of an interaction of CT DNA with the complexes; such interaction may result in the formation of a new conjugate between CT DNA and the complex understudy which seems to stabilize the CT DNA double-helix.

The changes of the absorption bands in the UV spectra of complexes **1–4** were studied in presence of a CT DNA solution at increasing amounts. More specifically, in the UV–vis spectra of complex **2**, both intraligand bands located at 298 nm and 419 nm exhibit in the presence of CT DNA a significant hyporchromism (Fig. 4(B)). Quite similar features are observed for the intraligand bands of complexes **1**, **3** and **4** (Table 2). The findings from UV–vis spectroscopy do not provide a clear indication concerning the DNA-binding mode of the compounds, since the extent of hypochromism is not so pronounced [74,75]. Therefore, DNA-viscosity measurements are necessary in order to clarify the DNA-binding mode.

The DNA-binding constants (K_b) of the compounds as calculated by the Wolfe-Shimer equation (Eq. S1) [58] and the plots [DNA] / ($\varepsilon_A - \varepsilon_f$) *versus* [DNA] (Fig. S11) are summarized in Table 2. The K_b values of the complexes are significantly higher than that of free HL suggesting stronger binding to DNA, and are higher than that of the classical intercalator (K_b = 1.23 × 10^5 M^{-1}) [76], with complex **2** showing the highest K_b constant among the compounds.

Table 2
UV–vis spectral data of the interaction of HL and complexes **1–4** with CT DNA. UV-band (λ in nm) (percentage of the observed hyper−/hypo-chromism (ΔA/A_o, %), blue−/red-shift of the λ_{max} (Δλ, nm)) and DNA-binding constants (K_b).

Compound	λ (nm) (ΔA/A_o(%),[a] Δλ (nm)[b])	$K_b(M^{-1})$
HL	330 (−4.8,[a] 0); 405(sh) (−3, 0)	8.38(± 0.70) × 10^4
$[Cu(L)(H_2O)_2](NO_3)$, **1**	401(−17, 0)	3.30(± 0.22) × 10^5
$[Cu(L)_2]$, **2**	298(−6.0, −1[b]); 419(−11.5, +3[b])	1.85(± 0.09) × 10^6
$[Ni(L)_2]$, **3**	302(−6.0, −3); 418(−3.0, −1)	1.21(± 0.12) × 10^5
$[Zn(L)_2]$, **4**	268 (+4,[a] +3); 338(−13, +8)	1.40(± 0.09) × 10^6

[a] "+" shows hyperchromism, "−"shows hypochromism.
[b] "+" shows red-shift, "−"shows blue-shift.

3.4.2. CT DNA-binding study with cyclic voltammetry

The interaction of metal complexes with DNA may be also studied by cyclic voltammetry; it is an electrochemical technique that provides useful information concerning the mode and the strength of interaction with both the reduced and oxidized form of the metal. The changes observed at the cyclic voltammograms of the complexes in the presence of DNA may be indicative of an interaction between the compounds and DNA [59]. In general, when the metal complex binds to DNA *via* intercalation, a positive shift of the electrochemical potential appears, while, in the case of electrostatic binding, the potential will shift to negative values. Furthermore, a positive shift of $E_{p,1}$ accompanied by a

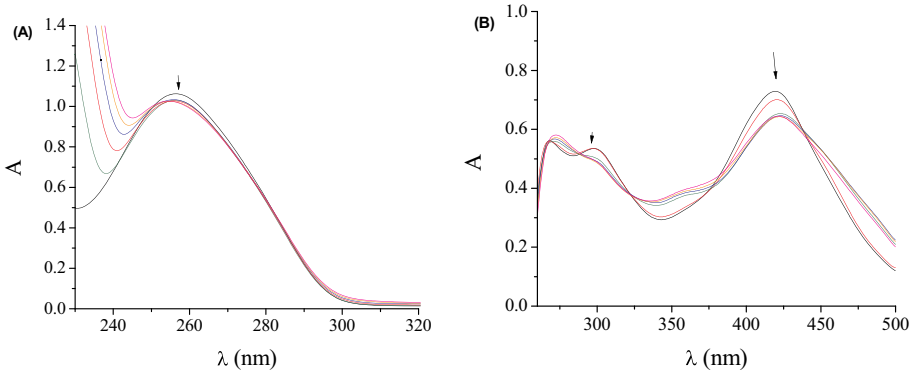

Fig. 4. UV–vis spectra of a: (A) buffer solution (15 mM trisodium citrate and 150 mM NaCl at pH 7.0) of CT DNA (1.6 × 10^{-4} M) in the presence of increasing amounts of complex **3**. The arrow shows the changes upon increasing amounts of the complex; (B) DMSO solution of complex **2** (2.5 × 10^{-5} M), in the presence of increasing amounts of CT DNA. The arrows show the changes upon addition of increasing amounts of CT DNA.

Table 3
Cathodic and anodic potentials (in mV) for the redox couple M(II)/M(I) of complexes **1–3** in 1/2 DMSO/buffer solution in the absence or presence of CT DNA. Ratio of equilibrium binding constants, K_r/K_{ox}.

Compound	$E_{pc(f)}$ [a]	$E_{pc(b)}$ [b]	ΔE_{pc} [c]	$E_{pa(f)}$ [a]	$E_{pa(b)}$ [b]	ΔE_{pa} [c]	K_r/K_{ox}
$[Cu(L)(H_2O)_2](NO_3)$, **1**	−710	−670	+40	−340	−440	−100	0.60
$[Cu(L)_2]$, **2**	−715	−705	+10	−496	−492	+4	1.13
$[Ni(L)_2]$, **3**	−715	−685	+30	−436	−450	−14	1.15

[a] $E_{pc/a}$ in DMSO/buffer in the absence of CT DNA ($E_{pc/a(f)}$).
[b] $E_{pc/a}$ in DMSO/buffer in the presence of CT DNA ($E_{pc/a(b)}$).
[c] $\Delta E_{pc/a} = E_{pc/a(b)} - E_{pc/a(f)}$.

simultaneous negative shift of $E_{p,2}$ may imply that the molecule may interact with DNA by both ways [77].

The cyclic voltammogramms of complexes **1–3** in a 1/2 DMSO/buffer solution were recorded in the absence and presence of CT DNA (representatively shown for **3** in Fig. S12) and the shifts of the corresponding cathodic (E_{pc}) and anodic (E_{pa}) potentials of the complexes are cited in Table 3. For all complexes, a positive shift of the potential (s) is evidence of the existence of an intercalative interaction with CT DNA. Especially for complex **1**, the intense negative shift of the anodic potential may reveal the co-existence of electrostatic interactions between the cationic complex **1** and the anionic phosphate groups of CT DNA, which is usually expected for cationic compounds.

Furthermore, the ratio of the corresponding equilibrium DNA-binding constants for the reduced form (K_r) and oxidized forms (K_{ox}) of the complexes (K_r/K_{ox}) was determined with Eq. S2 [59]. For complexes **2** and **3**, the ratio K_r/K_{ox} is in the range 1.13–1.15 (Table 3) which shows stronger binding of CT DNA with the reduced form of the complexes than its oxidized form, while for complex **1** the value of K_r/K_{ox} = 0.60 shows the opposite tendency [78].

3.4.3. CT DNA-binding study with viscosity measurements

The measurement of the viscosity of a DNA solution in the presence of the DNA-interacting compounds may provide additional information for the interaction of the compounds with CT DNA. The relative DNA-viscosity will show an increase in the case of intercalation, while in the case of nonclassical intercalation i.e. groove-binding or electrostatic interaction, it will decrease slightly or remain unchanged [79].

In the presence of increasing amounts of complexes **1–4**, the viscosity of a DNA solution (0.1 mM) showed a considerable increase (Fig. 5(A)), which may be due to the existence of intercalation of the compounds to the DNA. When an intercalating compound inserts in-between the DNA-bases, there are longer separation distances between them inducing an increase of the relative DNA-length and subsequent increase of DNA-viscosity. According to the aforementioned, intercalation is the most likely way of interaction between complexes **1–4** and CT DNA. Especially for complexes **2** and **4**, the increase of DNA-viscosity is more pronounced in agreement with their DNA-binding constants, since they have the highest K_b values among the compounds under study (Table 2). In the case of HL, the DNA-viscosity decreased slightly showing a nonclassical intercalation, i.e. external interaction.

3.4.4. Competitive study with EB

EB is a typical DNA-intercalator since the planar EB-phenanthridine ring inserts in-between DNA-bases forming an EB-DNA conjugate. The solution containing this EB-DNA conjugate, results in the appearance of an intense fluorescence emission band at 592 nm, when the EB-DNA solution is excited at 540 nm. The co-existence of an intercalating compound in this solution is potent to compete with EB and displace it from EB-DNA conjugate and will probably induce a quenching of this emission band [60,80]. The ability of the complexes to displace the typical DNA-intercalator EB from its EB-DNA complex was employed with fluorescence emission spectroscopy.

Upon addition of the compounds at increasing *r* values (up to *r* = 0.5, representatively shown for complex **1** in Fig. 5(B)) into a pretreated solution of EB-DNA, a remarkable quenching of the emission band of the DNA-EB system at 592 nm appeared (up to ~70% of the initial EB-DNA fluorescence, Fig. S13, Table 4). The observed quenching of CT DNA-EB fluorescence may be ascribed to the displacement of EB the compounds, especially by complexes **1–4**, in accordance to the linear Stern-Volmer equation (Eq. S3) and the corresponding Stern-Volmer plots (Fig. S14, *R* = 0.99), and may reveal indirectly the interaction with CT DNA by intercalation [60,80].

The values of the K_{sv} of the complexes (Table 4) are high enough to validate their ability to bind tightly to CT DNA. The values of K_{sv} of the complexes are higher than the free HL, while complexes **2** and **3** exhibit the highest K_{sv} value (= 2.83–2.87 × 10^5 M^{-1}) among the compounds under study. The determined k_q constants are significantly higher than the value of 10^{10} M^{-1} s^{-1} [62] suggesting that the quenching of the EB-DNA fluorescence from the complexes takes place *via* a static mechanism leading to the formation of a new conjugate between CT DNA and the compounds [60].

3.5. Interaction of the compounds with pBR322 plasmid DNA

3.5.1. DNA-cleavage activity of the compounds

DMSO solutions of HL and its complexes **1–4** (500 μM and 300 μM) were mixed with a Tris buffer solution (25 μM, pH = 6.8) containing the supercoiled circular pBR322 plasmid DNA (Form I). Plasmid DNA was analyzed by gel electrophoresis on 1% agarose stained with EB. All

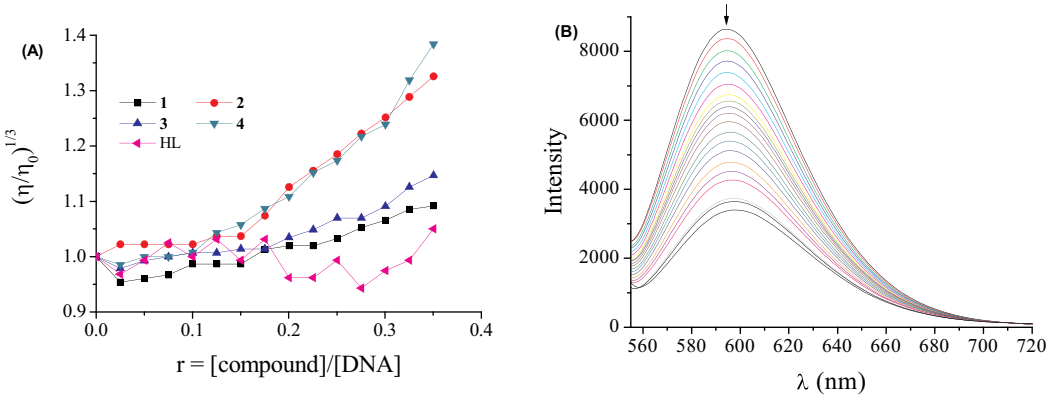

Fig. 5. (A) Relative viscosity of CT DNA $(\eta/\eta_o)^{1/3}$ in buffer solution (150 mM NaCl and 15 mM trisodium citrate at pH 7.0) in the presence of HL and complexes **1–4** at increasing amounts (r = [complex]/[DNA]). (B) Fluorescence emission spectra (λ_{ex} = 540 nm) for EB-DNA ([EB] = 20 μM, [DNA] = 26 μM) in buffer solution (150 mM NaCl and 15 mM trisodium cictrate at pH 7.0) in the absence and presence of increasing amounts of complex **1**. The arrow shows the changes of intensity upon increasing amounts of **1**.

Table 4
Percentage of EB-DNA fluorescence quenching (ΔI/Io, %), Stern-Volmer constants (K_{SV}, in M^{-1}) and quenching constants of the EB-DNA fluorescence (k_q, in $M^{-1}\ s^{-1}$) for HL and complexes **1–4**.

Compound	ΔI/Io (%)	$K_{sv}(M^{-1})$	$k_q(M^{-1}\ s^{-1})$
HL	59.5	$6.02(\pm 0.08) \times 10^4$	$2.62(\pm 0.03) \times 10^{12}$
$[Cu(L)(H_2O)_2](NO_3)$, **1**	61.6	$2.52(\pm 0.06) \times 10^5$	$1.10(\pm 0.03) \times 10^{13}$
$[Cu(L)_2]$, **2**	69.1	$2.87(\pm 0.10) \times 10^5$	$1.25(\pm 0.05) \times 10^{13}$
$[Ni(L)_2]$, **3**	63.7	$2.83(\pm 0.12) \times 10^5$	$1.23(\pm 0.05) \times 10^{13}$
$[Zn(L)_2]$, **4**	69.3	$2.10(\pm 0.06) \times 10^5$	$9.14(\pm 0.26) \times 10^{12}$

experiments were performed at least three times. As shown in Fig. 6, the cleavage activity of most compounds at both concentrations tested is almost negligible since the percentage of generation of the relaxed circular DNA (Form II) is, in general, significantly low, while any sign of linear DNA was not observed. Complex **2** is the only active compound at 500 μM since its presence induces a 42% of relaxed DNA (form II).

3.5.2. DNA photo-cleavage activity of the compounds

DMSO solutions (500 μM and 300 μM) of HL and its complexes **1–4** were mixed with a Tris buffer solution (25 μM, pH = 6.8) containing the supercoiled circular pBR322 DNA (Form I). This mixture was irradiated at room temperature with UVB light (312 nm) for 30 min or UVA light (365 nm) for 2 h or visible light (400–800 nm) for 2 h, under aerobic conditions (Fig. 7). All compounds showed at least some UV absorption at the area of irradiation. Plasmid DNA was analyzed by gel electrophoresis on 1% agarose stained with EB. All experiments were performed at least three times.

The irradiation of the DNA-compound mixture with light at 312 nm, 365 nm and visible light has resulted in the generation of the relaxed circular DNA (Form II) and the linear DNA (Form III). In all cases, the complexes exhibit higher DNA-cleavage activity than free HL which arises up to 90% (= ss% + ds%) for complex **4** after irradiation at 365 nm and visible light.

As it can be seen, all complexes are active in all tested light wavelengths. Due to the better absorption at wavelengths higher than 350 nm, DNA photo-cleavage of all complexes was better at UVA and visible light (Fig. 7(B) and 7(C), respectively). At the concentration of 500 μM, three complexes, i.e. **1**, **3** and **4**, exhibited excellent activity, consuming all plasmid DNA and converting it into nicked (Form II) as well as into linear DNA (Form III), Fig. 7(B) and 7(C), lanes 4, 6, 7, respectively). Additionally, at lower concentrations the reactivity has dropped down in all except for complex **2.**

Among the four complexes, Zn complex has overall the best profile. The activity remains very high producing linear plasmid DNA at high percentage both at 500 and 300 μM, (lanes 7 and 12 in Fig. 7(A)-(C)) indicating that this compound should be powerful even at much lower concentrations, comparing to the rest three.

In total, complexes **1** and **3** are very good DNA-cleavagers at concentration 500 μM upon irradiation with UVB and UVA light, whereas complex **4** is the most active of all compounds tested for all lights and concentrations used.

3.6. Albumin-binding properties of the compounds

3.6.1. Interaction of the compounds with BSA - HSA

Serum albumin (SA) is the most important and abundant protein in blood serum since it is a multifunctional protein involved in the maintenance of the osmotic pressure in blood and of the acid-basis equilibrium [81]. Although albumin may possess anti-coagulant and antioxidant properties, one of its main roles is as carrier of compounds, such as hormones, fatty acids, ions and drugs that are poorly dissolved in water [81,82]; therefore, albumins may have wide clinical, pharmaceutical, and biochemical applications [83,84]. HSA and its homologue BSA are the most studied serum albumins in regard to their binding with bioactive compounds [85]. The solutions of both SAs exhibit an intense emission band located at $\lambda_{em,max}$ = 343 nm for BSA and 339 nm for HSA, when excited at 295 nm, due to the presence of tryptophan residues, i.e. the Trp-214 in sub-domain IIA for HSA and, the Trp-134 and Trp-212 in the first sub-domain IB and sub-domain IIA, respectively, for BSA [85,86].

The result of the addition of the compounds in the SA-solution was a significant quenching of the SA fluorescence emission band up to 78% of the initial fluorescence (representative spectra are shown in Fig. 8). Especially for complexes **2–4**, a second emission band appeared at 435–440 nm, followed by an isoemissive point at ~395 nm (Fig. 8(B)). Furthermore, the inner-filter effect was evaluated with Eq. S5; it was found too negligible to affect the measurements [64].

The observed quenching of the SA emission band resulted from the addition of the compounds (Fig. 9) was moderate in the case of HL (the quenching of the initial SA fluorescence emission (ΔI/Io) was up to ~68%) and more enhanced in the case of the complexes (up to ~78% in the presence of complex **4**). Such high quenching is usually attributed to possible changes around SA-tryptophan residues resulting from changes in albumin secondary structure due to the binding of the compounds to SA [87].

The quenching constants (k_q) concerning the interaction of the compounds with the SAs were determined (Table 5) with the Stern–-Volmer quenching equation (Eqs. S3 and S4, the fluorescence lifetime of tryptophan in SA is $\tau_o = 10^{-8}$ s [65]), and from the corresponding Stern-Volmer plots (Figs. S15 and S16). The obtained k_q constants are of the order $10^{13}\ M^{-1}\ s^{-1}$ and are significantly higher than $10^{10}\ M^{-1}\ s^{-1}$ indicating the existence of a static quenching mechanism [88] and subsequently verifying the interaction of the compounds complexes with SAs. The k_q constants may suggest that the compounds have significant SA-quenching ability; the k_q constants of the complexes are higher than that of free HL with complex **4** presenting the highest k_q constants for both SAs.

The values of the SA-binding constants (K) of the compounds were calculated with Scatchard equation (Eq. S6) and plots (Figs. S17 and

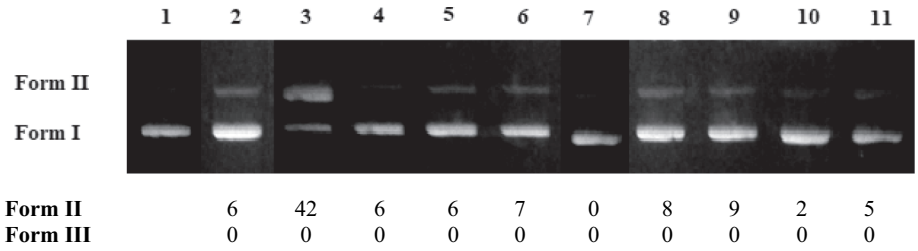

Form II	6	42	6	6	7	0	8	9	2	5
Form III	0	0	0	0	0	0	0	0	0	0

Fig. 6. Agarose gel electrophoretic pattern of EB-stained plasmid DNA (pBR322 plasmid DNA) with HL and complexes **1–4** at 500 μM (lanes 2–6) and 300 μM (lanes 7–11), after 30 min of electrophoresis. Gel electrophoreses pictures, Top: Lane 1: DNA; Lane 2–5: DNA + complexes **1–4** (500 μM); Lane 6: DNA + HL (500 μM); Lane 7–10: DNA + complexes **1–4** (300 μM); Lane 11: DNA + HL (300 μM); Bottom: Calculation of the % conversion to ss and ds damage. DNA forms: Form I = supercoiled and Form II = relaxed plasmid DNA.

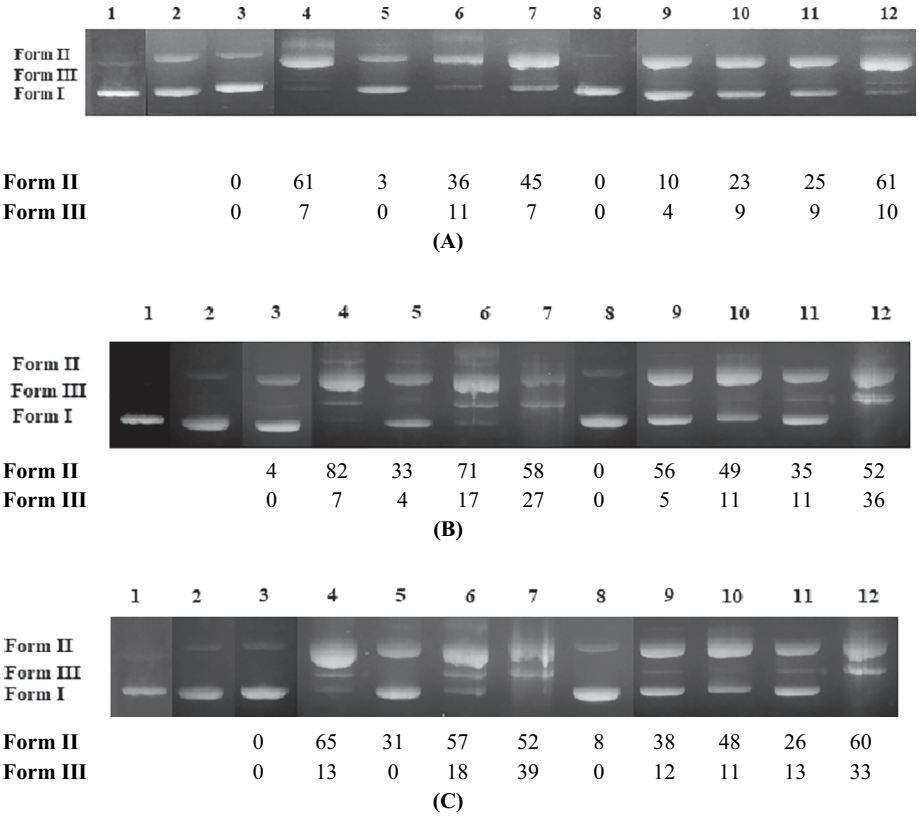

Fig. 7. DNA (pBR322 plasmid DNA) photo-cleavage of HL and complexes **1–4** at 500 μM (lanes 3–7) and 300 μM (lanes 8–12) with irradiation at: (A) 312 nm, (B) 365 nm and (C) visible. Gel electrophoreses pictures, Top: Lane 1: DNA without irradiation; Lane 2: DNA with irradiation; Lane 3: DNA + HL (500 μM) + irradiation; Lane 4–7: DNA + complexes **1–4** (500 μM) + irradiation; Lane 8: DNA + HL (300 μM) + irradiation; Lane 9–12: DNA + complexes **1–4** (300 μM) + irradiation; Bottom: Calculation of the % conversion to ss and ds damage. DNA forms: Form I = supercoiled, Form II = relaxed, Form III = linear plasmid DNA.

S18). The compounds present are relatively high (of the order 10^4–10^5 M^{-1}) with the complexes being better SA-binders than HL. In addition, the magnitude of the K values of the compounds (2.04×10^4–3.18×10^5 M^{-1}) may indicate their tight and reversible binding to albumins. The K constants are relatively high showing their binding to albumin and the potential to be carried through the bloodstream but also relatively low (lower than $K \approx 10^{15}$ M^{-1} which is the limit value for the strongest known non-covalent interactions, i.e. avidin with diverse ligands) and can get released upon arrival at the desired biotargets [89].

3.6.2. Location of the SA-binding site

The albumins have been crystallographically characterized. They consist of three domains (I, II and III) which are divided in two subdomains (A and B) [90]. There are at least four sites in the albumin where drugs and metal ions can be bound. The most important sites where drugs are bound are Sudlow's site 1 (or drug site I) located in subdomain IIA and Sudlow's site 2 (or drug site II) located in subdomain IIIA [90]. Warfarin and ibuprofen are the most common markers of the SA-binding site, since they show high binding affinity for sites I and II, respectively [91].

The SA-subdomain where HL and complexes **1–4** may bind to BSA or HSA can be specified by competitive experiments with warfarin and ibuprofen by fluorescence emission spectroscopy. The addition of HL and complexes **1–4** to a pre-treated solution containing SA and the site-probe resulted in a significant quenching of the initial fluorescence emission band (Figs. 10 and 11).

The SA-binding constants of the complexes in the presence of warfarin or ibuprofen were calculated with the Scatchard equation (Eq. S6) and plots (Figs. S19–S22) and their values are given in Table 6. These values are compared with those determined in the absence of any site-marker (Table 6); a decrease of the value of K in presence of the site-

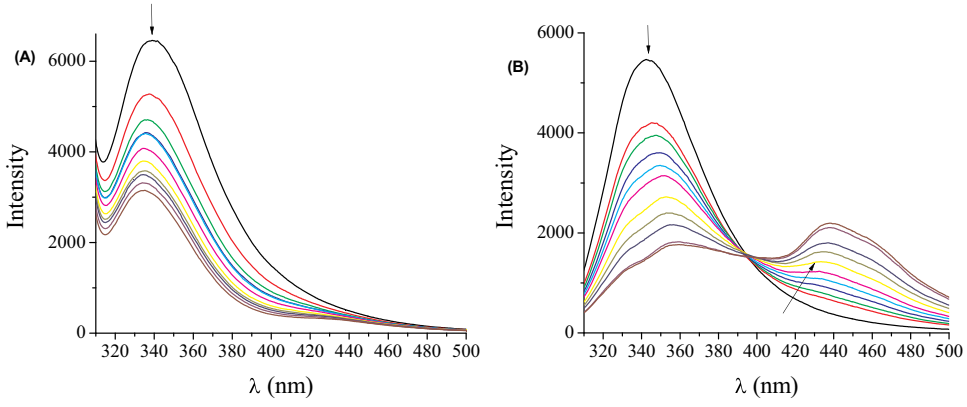

Fig. 8. (A) Fluorescence emission spectra ($\lambda_{excitation}$ = 295 nm) for HSA ([HSA] = 3 μM) in buffer solution (150 mM NaCl and 15 mM trisodium citrate at pH 7.0) in the absence and presence of increasing amounts of complex **1**. The arrow shows the changes of intensity upon increasing amounts of **1**. (B) Fluorescence emission spectra ($\lambda_{excitation}$ = 295 nm) for BSA ([BSA] = 3 μM) in buffer solution (150 mM NaCl and 15 mM trisodium citrate at pH 7.0) in the absence and presence of increasing amounts of complex **4**. The arrows show the changes of intensity upon increasing amounts of **4**.

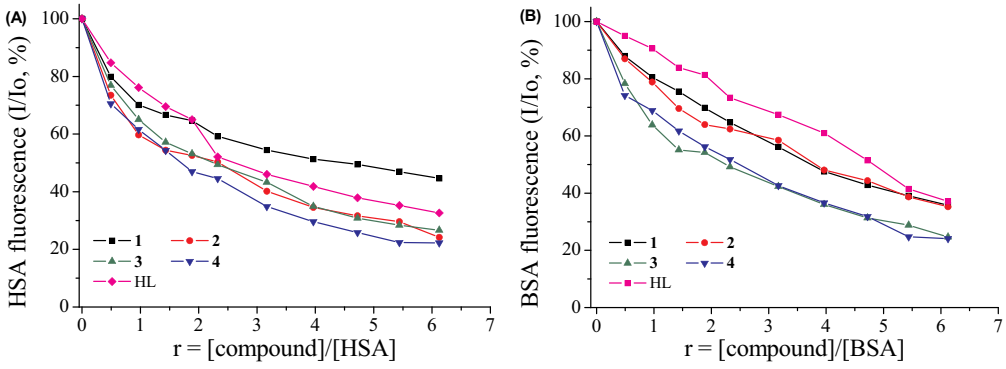

Fig. 9. (A) Plot of % relative fluorescence intensity at λ_{em} = 339 nm (I/Io, %) versus *r* (*r* = [complex]/[HSA]) for HL and complexes **1–4** (up to 44.6% of the initial BSA fluorescence for **1**, 24.2% for **2**, 26.6% for **3**, 22.3% for **4**, and 32.6% for HL) in buffer solution (150 mM NaCl and 15 mM trisodium citrate at pH 7.0). (B) Plot of % relative fluorescence intensity at λ_{em} = 343 nm (I/Io, %) versus *r* (*r* = [complex]/[BSA]) for HL and complexes **1–4** (up to 35.8% of the initial BSA fluorescence for **1**, 35.2% for **2**, 24.7% for **3**, 24.1% for **4**, and 37.1% for HL) in buffer solution (150 mM NaCl and 15 mM trisodium citrate at pH 7.0).

marker shows that the binding of the compound to albumin is influenced by the presence of this marker due to competition for the same binding site [91].

More specifically, the BSA-binding constants of HL and complexes **1–3** decreased significantly in the presence of ibuprofen, suggesting that the most possible binding site of the compounds to BSA is Sudlow's site 2 in subdomain IIIA. For HSA, the binding HSA-binding constants decreased in almost all cases; for HL and complexes **1** and **4**, the most remarkable decrease was observed in the presence of ibuprofen suggesting their preference for Sudlow's site 2 in subdomain IIIA, while complexes **2** and **3** seem to prefer is Sudlow's site 1 in subdomain IIA, since they have shown higher decrease of HSA-binding in presence of warfarin [91,92]. In average, the compounds seem to prefer to bind to BSA at Sudlow's site 2, while for HSA there is not such a discrete tendency of preferential binding site.

3.7. Radical scavenging activity of the compounds

Free radicals are species responsible for the inflammations [93]. Antioxidants help the neutralization of free oxygen radicals, which attack cells by causing or accelerating natural processes such as aging, as well as the occurrence of chronic diseases such as heart disease and cancer. Compounds that can scavenge free radicals or inhibit their production may be a useful tool in the treatment of inflammations. Since quinazolinones are used as anti-inflammatory agents [94–96], we have investigated the *in vitro* ability of HL and its complexes **1–4** to scavenge DPPH and ABTS radicals. The scavenging activity of complexes **1–4** was compared with that of the most commonly used as reference antioxidant agents, NDGA, BHT and trolox, and the results are summarized in Table 7.

DPPH-scavengers often provide potential antiageing, anticancer and anti-inflammatory activity [93]. The DPPH-scavenging ability of HL and complexes **1**, **2** and **4** was found time-independent, while for complex **3** the DPPH-scavenging activity increased noteworthy upon time. In addition, complexes **2–4** were much more active than free HL. HL and complexes **1–3** present low-to-moderate ability to scavenge DPPH radicals, when compared to the reference compounds and complex **4**. Complex $[Zn(L)_2]$ **4** shows the highest DPPH-scavenging activity among the complexes and may be considered a good DPPH-scavenger, even more active than the reference compound BHT. Analogous DPPH-scavenging activity was found for a series of metal complexes (Mn(II) and Zn) of the non-steroidal anti-inflammatory drug oxaprozin [97,98].

ABTS radical scavengers ($ABTS^{+\cdot}$) often serve as markers of the total antioxidant activity [93]. Complexes **1–4** are more active ABTS-scavengers than free HL but less active than the reference compound trolox. Complex **4** is the best ABTS-scavenger among the compounds under study with similar ABTS-scavenging ability with trolox.

In conclusion, complexes **1–4** are more potent radical scavengers than the free HL, indicating that enhanced scavenging activity towards DPPH and ABTS radicals may result from its coordination to metals; such result is in accordance with reports where the metal complexes of bioactive ligands were more active radical scavengers than the corresponding free ligands. In addition, the complexes seem to show selective scavenging activity of ABTS towards DDPH.

4. Conclusions

The reaction of the novel guanine-based 2-hydrazinyl-4(3H)-quinazolinone derivative (HL) with Cu(II) in a 1:1 M:L ratio resulted in the formation of the cationic complex $[Cu(L)(H_2O)_2](NO_3)$, **1** which was characterized by single-crystal X-ray crystallography. When a 1:2 M:L ratio was applied for the reaction of HL with Cu(II), Ni(II) and Zn(II), the neutral complexes of the formula $[M(L)_2]$ (M = Cu for **2**, Ni for **3** and Zn for **4**) was isolated. The characterization of all complexes was accomplished by a series of spectroscopic techniques, including HRMS, IR, UV–vis and ^{1}H NMR spectroscopies. In all complexes, the ligand L is bound to the metal in a tridentate fashion *via* the pyridine nitrogen, the hydrazine nitrogen and the quinazoline nitrogen atoms.

The interaction of compounds with CT DNA was investigated by diverse techniques. All complexes **1–4** may bind to CT *via* intercalation, while for complex **1** the possibility of electrostatic interactions with CT has been also revealed. Complexes **2** and **4** seem to bind more tightly to CT DNA than the other two complexes since they present the highest DNA-binding constants.

The ability of the compounds to induce cleavage to the supercoiled circular pBR322 plasmid DNA was investigated by agarose gel

Table 5
The SA-quenching (k_q) and SA-binding (K) constants for HL and complexes **1–4**.

Compound	$k_{q(HSA)}$ (M^{-1} s^{-1})	$K_{(HSA)}$ (M^{-1})	$k_{q(BSA)}$ (M^{-1} s^{-1})	$K_{(BSA)}$ (M^{-1})
HL	1.15(± 0.02) × 10^{13}	9.98(± 0.36) × 10^4	5.48(± 0.23) × 10^{12}	2.04(± 0.08) × 10^4
$[Cu(L)(H_2O)_2](NO_3)$, **1**	5.75(± 0.17) × 10^{12}	3.02(± 0.12) × 10^5	9.83(± 0.29) × 10^{12}	5.23(± 0.17) × 10^4
$[Cu(L)_2]$, **2**	1.42(± 0.05) × 10^{13}	3.18(± 0.11) × 10^5	9.60(± 0.30) × 10^{12}	1.02(± 0.06) × 10^5
$[Ni(L)_2]$, **3**	1.50(± 0.03) × 10^{13}	2.11(± 0.07) × 10^5	1.47(± 0.04) × 10^{13}	2.14(± 0.09) × 10^5
$[Zn(L)_2]$, **4**	2.05(± 0.06) × 10^{13}	2.05(± 0.06) × 10^5	1.65(± 0.08) × 10^{13}	1.17(± 0.06) × 10^5

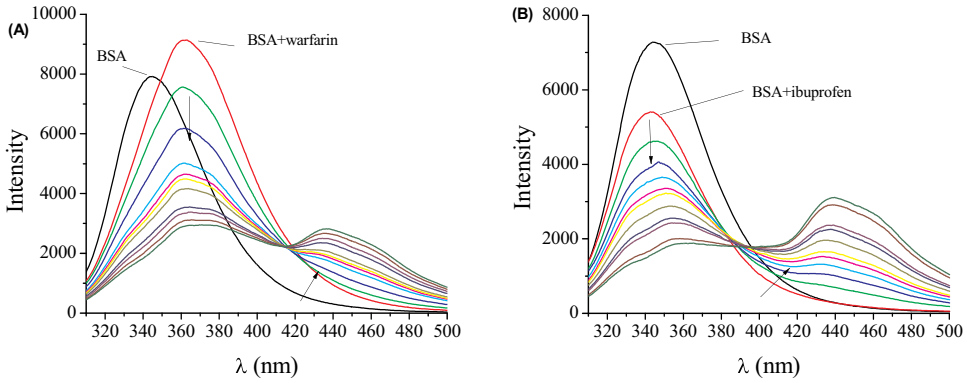

Fig. 10. (A) Fluorescence emission spectra ($\lambda_{excitation}$ = 295 nm) for BSA (3 μM) in the presence of warfarin (3 μM) in buffer solution (150 mM NaCl and 15 mM trisodium citrate at pH 7.0) upon addition of increasing amounts of complex **4**. The arrow shows the changes of intensity upon increasing amounts of **4**. (B) Fluorescence emission spectra ($\lambda_{excitation}$ = 295 nm) for BSA (3 μM) in the presence of ibuprofen (3 μM) in buffer solution (150 mM NaCl and 15 mM trisodium citrate at pH 7.0) upon addition of increasing amounts of complex **4**. The arrows show the changes of intensity upon increasing amounts of **4**.

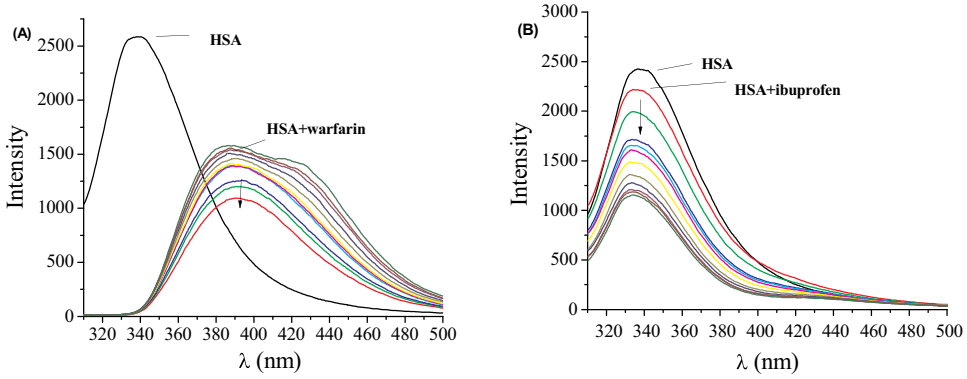

Fig. 11. (A) Fluorescence emission spectra ($\lambda_{excitation}$ = 295 nm) for HSA (3 μM) in the presence of warfarin (3 μM) in buffer solution (150 mM NaCl and 15 mM trisodium citrate at pH 7.0) upon addition of increasing amounts of complex **1**. The arrow shows the changes of intensity upon increasing amounts of **1**. (B) Fluorescence emission spectra ($\lambda_{excitation}$ = 295 nm) for HSA (3 μM) in the presence of ibuprofen (3 μM) in buffer solution (150 mM NaCl and 15 mM trisodium citrate at pH 7.0) upon addition of increasing amounts of complex **1**. The arrows show the changes of intensity upon increasing amounts of **1**.

electrophoresis experiments. The effect of the concentration of the compounds used and of the irradiation with diverse lights has been also taken into consideration. In absence of any irradiation, complex **1** was the only (most) active compound at concentration of 500 μM inducing a relatively high cleavage of DNA. Upon irradiation, the DNA-cleavage for all compounds was much more intense and they showed their relatively high potency to cleave supercoiled circular DNA towards relaxed DNA and in some case, especially upon irradiation with light at 365 nm or visible light, the linear DNA was also observed. In average, complexes **1**, **3** and **4** were more active at concentration of 500 μM, and complex **4** at 300 μM and below. Such activity is interesting and promising for any potential application of the compounds in photodynamic therapy.

The ability of the compounds to bind to BSA and HSA was also investigated. The compounds can bind tightly and reversibly to these albumins in order to get transferred towards potential biological targets. In addition, the SA-binding site of the compounds was investigated *via* competitive studies with the typical site-probes warfarin and ibuprofen. Most of the present compounds prefer to bind to BSA at Sudlow's site 2 in subdomain IIIA, in competition to ibuprofen. For HSA, HL, **1** and **4**, have shown their preference for Sudlow's site 2 in

Table 7
% DPPH-scavenging ability (DPPH%) and % ABTS radical scavenging activity (ABTS%) for HL and its complexes **1**–**4**.

Compound	DPPH%, 30 min	DPPH%, 60 min	ABTS%
HL	10.24 ± 0.72	18.27 ± 0.59	7.07 ± 0.25
$[Cu(L)(H_2O)_2](NO_3)$, **1**	7.53 ± 0.37	10.43 ± 0.21	66.46 ± 0.45
$[Cu(L)_2]$, **2**	17.85 ± 0.21	17.66 ± 0.79	56.45 ± 0.62
$[Ni(L)_2]$, **3**	32.68 ± 0.22	42.24 ± 0.43	62.12 ± 1.16
$[Zn(L)_2]$, **4**	76.08 ± 0.22	79.29 ± 0.53	98.19 ± 0.14
NDGA	87.08 ± 0.12	87.47 ± 0.12	Not tested
BHT	61.30 ± 1.16	76.78 ± 1.12	Not tested
Trolox	Not tested	Not tested	98.10 ± 0.48

All measurements were carried out in triplicate.

Table 6
SA-binding constants of the compounds (K, in M^{-1}) in the absence or presence of the site probes warfarin and ibuprofen.

Compound	No probe	Probe: warfarin	Probe: ibuprofen
BSA			
HL	$2.04(\pm 0.08) \times 10^4$	$1.57(\pm 0.07) \times 10^5$	$1.15(\pm 0.04) \times 10^5$
$[Cu(L)(H_2O)_2](NO_3)$, **1**	$5.23(\pm 0.17) \times 10^4$	$1.33(\pm 0.05) \times 10^5$	$4.77(\pm 0.28) \times 10^4$
$[Cu(L)_2]$, **2**	$1.02(\pm 0.06) \times 10^5$	$2.25(\pm 0.09) \times 10^5$	$5.38(\pm 0.16) \times 10^4$
$[Ni(L)_2]$, **3**	$2.14(\pm 0.09) \times 10^5$	$2.22(\pm 0.08) \times 10^5$	$9.69(\pm 0.35) \times 10^4$
$[Zn(L)_2]$, **4**	$1.17(\pm 0.06) \times 10^5$	$2.45(\pm 0.06) \times 10^5$	$1.56(\pm 0.07) \times 10^5$
HSA			
HL	$9.98(\pm 0.36) \times 10^4$	$8.27(\pm 0.52) \times 10^4$	$5.94(\pm 0.24) \times 10^4$
$[Cu(L)(H_2O)_2](NO_3)$, **1**	$3.02(\pm 0.12) \times 10^5$	$1.88(\pm 0.09) \times 10^5$	$1.15(\pm 0.03) \times 10^5$
$[Cu(L)_2]$, **2**	$3.18(\pm 0.11) \times 10^5$	$4.19(\pm 0.37) \times 10^4$	$1.24(\pm 0.06) \times 10^5$
$[Ni(L)_2]$, **3**	$2.11(\pm 0.07) \times 10^5$	$5.10(\pm 0.06) \times 10^4$	$8.83(\pm 0.27) \times 10^4$
$[Zn(L)_2]$, **4**	$2.05(\pm 0.06) \times 10^5$	$2.43(\pm 0.05) \times 10^5$	$1.75(\pm 0.07) \times 10^5$

subdomain IIIA, and complexes **2** and **3** seem to prefer Sudlow's site 1 in subdomain IIA, in competition to warfarin.

The scavenging activity of the compounds towards DPPH and ABTS radicals was noteworthy. The scavenging activity of complex **4** towards both radicals tested was significantly high and comparable to the reference compounds.

In conclusion, the herein presented biological properties of complexes **1–4** with the novel HL are promising for potential applications and further studies may be conducted.

Declaration of competing interest

There are no conflicts to declare.

Acknowledgements

This research is carried out/funded in the context of the project "Novel guanine-based derivatives of 2-hydrazido-4(3H)-quinazolinone and their transition metal complexes: Synthesis, structure and biological activity" (MIS 5004526) under the call for proposals "Supporting researchers with emphasis on new researchers" (EDULLL 34). The project is co-financed by Greece and the European Union (European Social Fund-ESF) by the Operational Programme Human Resources Development, Education and Lifelong Learning 2014–2020.

The aid of Professor Konstantina C. Fylaktakidou, (Molecular Biology and Genetics Department, Democritus University of Thrace, Alexandroupolis, Greece, and Laboratory of Organic Chemistry, Department of Chemistry, Aristotle University of Thessaloniki, Greece) for the synthesis and characterization of the organic compounds was valuable. The authors would like to thank Associate Professor Antonios Hatzidimitriou (Laboratory of Inorganic Chemistry, Department of Chemistry, Aristotle University of Thessaloniki, Greece) for his help with the X-ray structural characterization. We also owe thanks to Dr. M. Kokotou for performing HRMS analyses at the National and Kapodistrian University of Athens.

Abbreviations

ABTS	2,2′-azinobis-(3-ethylbenzothiazoline-6-sulfonic acid)
BHT	butylated hydroxytoluene
BSA	bovine serum albumin
CT	calf-thymus
DPPH	1,1-diphenyl-picrylhydrazyl
ds%	double-strand damage
EB	ethidium bromide
E_{pa}	anodic potential
E_{pc}	cathodic potential
HRMS	High resolution mass spectra
HSA	human serum albumin
K	SA-binding constant
K_b	DNA-binding constant
K_{ox}	DNA-binding constant for the oxidized form
k_q	quenching constant
K_r	DNA-binding constant for the reduced form
K_{SV}	Stern-Volmer constant
m	medium
NDGA	nordihydroguaiaretic acid
r	[compound]/[CT DNA] mixing ratio
s	strong
SA	serum albumin
sh	shoulder
ss%	single-strand damage
trolox	6-hydroxy-2,5,7,8-tetramethylchromane-2-carboxylic acid
vs	very strong
τ_o	fluorescence lifetime

Appendix A. Supplementary data

CCDC 1968944 contains the supplementary crystallographic data for this paper. These data can be obtained free of charge via www.ccdc.cam.ac.uk/conts/retrieving.html (or from the Cambridge Crystallographic Data Centre, 12 Union Road, Cambridge CB21EZ, UK; fax: (+44) 1223-336-033; or deposit@ccde.cam.ac.uk). Supplementary data associated with this article can be found, in the online version, at https://doi.org/10.1016/j.jinorgbio.2020.111019.

References

[1] H. Zhao, J. Dietrich, Expert Opin. Drug Discov. 10 (2015) 781–790.
[2] C.D. Duarte, E.J. Barreiro, C.A. Fraga, Mini Rev. Med. Chem. 7 (2007) 1108–1119.
[3] B.K. Tiwary, K. Pradhan, A.K. Nanda, R. Chakraborty, J. Chem. Biol. Ther. 104 (2015) 1–14 and references therein.
[4] E. Jafari, M.R. Khajouei, F. Hassanzadeh, G.H. Hakimelahi, G.A. Khodarahmi, Research in Pharmaceutical Sciences 11 (2016) 1–14.
[5] I. Khan, A. Ibrar, W. Ahmed, A. Saeed, Eur. J. Med. Chem. 90 (2015) 124–169.
[6] I. Khan, A. Ibrar, N. Abbas, A. Saeed, Eur. J. Med. Chem. 76 (2014) 193–244.
[7] I. Khan, S. Zaib, S. Batool, N. Abbas, Z. Ashraf, J. Iqbal, A. Saeed, Bioorg. Med. Chem. 24 (2016) 2361–2381.
[8] V. Alagarsamy, M. Gopinath, P. Parthiban, B. Subba Rao, K. Murali, V.R. Solomon, Med, Chem. Res. 20 (2011) 946–954.
[9] V. Alagarsamy, V. Raja Solomon, K. Dhanabal, Bioorg. Med. Chem. 15 (2007) 235–241.
[10] N. Saygili, M. Ekizoglu, C. Erdogdu, Asian J. Chem. 26 (2014) 3197–3203.
[11] K. Siddappa, S.B.Mane, D. Manikprabhu, The Scientific World Journal 2014 (2014) Article ID 817365.
[12] S. Thota, M. Imran, M. Udugula, S.S. Karki, N. Kanjarla, R. Yerra, J. Balzarini, E. De Clercq, J. Coord. Chem. 65 (2012) 823–839.
[13] K.S. Prasad, L.S. Kumar, S. Chandan, R.M. Naveen Kumar, H.D. Revanasiddappa, Spectrochim. Acta Part A 107 (2013) 108–116.
[14] K.S. Prasad, L.S. Kumar, S. Chandan, B. Jayalakshmi, H.D. Revanasiddappa, Spectrochim. Acta Part A 81 (2011) 276–282.
[15] P. Chellan, P.J. Sadler, Phil. Trans. Roy. Soc. A 373 (2015) 20140182.
[16] G. Crisponi, V.M. Nurchi, D. Fanni, C. Gerosa, S. Nemolato, G. Faa, Coord. Chem. Rev. 254 (2010) 876–889.
[17] W.X. Tian, S. Yu, M. Ibrahim, A.W. Almonaofy, L. He, Q. Hui, Z. Bo, B. Li, G.L. Xie, J. Microbiol. 50 (2012) 586–593.
[18] S. Medici, M. Peana, V.M. Nurchi, J.I. Lachowicz, G. Crisponi, M.A. Zoroddu, Coord. Chem. Rev. 284 (2015) 329–350.
[19] P. Fernandes, I. Sousa, L. Cunha-Silva, M. Ferreira, B. de Castro, E.F. Pereira, M.J. Feio, P. Gameiro, J. Inorg. Biochem. 131 (2014) 21–29.
[20] B. Chudzik, I.B. Tracz, G. Czernel, M.J. Fiolka, G. Borsuk, M. Gagos, Eur. J. Pharm. Sci. 49 (2013) 850–857.
[21] M. Gziut, H.J. MacGregor, T.G. Nevell, T. Mason, D. Laight, J.K. Shute, Br. J. Pharmacol. 168 (2013) 1165–1181.
[22] J. Nagaj, R. Starosta, M. Jezowska-Bojczuk, J. Inorg. Biochem. 142 (2015) 68–74.
[23] G.K. Walkup, S.C. Burdette, S.J. Lippard, R.Y. Tsien, J. Am. Chem. Soc. 122 (2000) 5644–5645.
[24] B.L. Vallee, D.S. Auld, Biochemistry 32 (1993) 6493–6500.
[25] C.P. Larson, U.R. Saha, H. Nazrul, PLoS Med. 6 (2009) e1000175.
[26] H. Sakurai, Y. Kojima, Y. Yoshikawa, K. Kawabe, H. Yasui, Coord. Chem. Rev. 226 (2002) 187–198.
[27] Q. Zhou, T.W. Hambley, B.J. Kennedy, P.A. Lay, P. Turner, B. Warwick, J.R. Biffin, H.L. Regtop, Inorg. Chem. 39 (2000) 3742–3748.
[28] A. Tarushi, K. Lafazanis, J. Klun, I. Turel, A.A. Pantazaki, G. Psomas, D.P. Kessissoglou, J. Inorg. Biochem. 121 (2013) 53–65.
[29] A. Tarushi, C. Kakoulidou, C.P. Raptopoulou, V. Psycharis, D.P. Kessissoglou, I. Zoi, A.N. Papadopoulos, G. Psomas, J. Inorg. Biochem. 170 (2017) 85–97.
[30] J.S. Casas, E.E. Castellano, M.D. Couce, J. Ellena, A. Sanchez, J. Sordo, C. Taboada, J. Inorg. Biochem. 100 (2006) 124–132.
[31] F. Meyer, H. Kozlowski, in: J.A. McCleverty, T.J. Meyer (Eds.), Comprehensive Coordination Chemistry II, Vol. 6, Elsevier, 2003, pp. 247–554.
[32] R.K. Andrews, R.L. Blakeley, B. Zerner, in: H. Sigel, A. Sigel (Eds.), Metal Ions in Biological Systems, 23 Marcel Dekker Inc., New York, 1988, pp. 165–284.
[33] Agency for Toxic Substances and Disease Registry (ATSDR), Toxicological profile for nickel. Atlanta, GA: U.S, Department of Health and Human Services, Public Health Service, 2005.
[34] C. Buttice, G.A. Colditz In (Eds.), The SAGE Encyclopedia of Cancer and Society, second ed., SAGE Publications, Inc., Thousand Oaks, 2015, pp. 828–831.
[35] N.E. Dixon, C. Gazzola, R.L. Blakeley, B. Zerner, J. Am. Chem. Soc. 97 (1975) 4131–4133.
[36] K.C. Skyrianou, E.K. Efthimiadou, V. Psycharis, A. Terzis, D.P. Kessissoglou, G. Psomas, J. Inorg. Biochem. 103 (2009) 1617–1625.
[37] B. Xu, P. Shi, Q. Guan, X. Shi, G. Zhao, J. Coord. Chem. 66 (2013) 2605–2614.
[38] K. Alomar, A. Landreau, M. Allain, G. Bouet, G. Larcher, J. Inorg. Biochem. 126 (2013) 76–83.
[39] H.B. Shawish, W. Wong, Y. Wong, S. Loh, C. Looi, P. Hassandarvish, A. Phan, W. Wong, H. Wang, I.C. Paterson, C. Ea, M. Mustafa, M. Maah, PLoS One 9 (2014) e100933.

[40] X. Totta, A.A. Papadopoulou, A.G. Hatzidimitriou, A. Papadopoulos, G. Psomas, J. Inorg. Biochem. 145 (2015) 79–93.
[41] S. Perontsis, A.G. Hatzidimitriou, A.N. Papadopoulos, G. Psomas, J. Inorg. Biochem. 162 (2016) 9–21.
[42] F. Bisceglie, S. Pinelli, R. Alinovi, M. Goldoni, A. Mutti, A. Camerini, L. Piola, P. Tarasconi, G. Pelosi, J. Inorg. Biochem. 140 (2014) 111–125.
[43] S. Betanzos-Lara, C. Gomez-Ruiz, L.R. Barron-Sosa, I. Gracia-Mora, M. Flores-Alamo, N. Barba-Behrens, J. Inorg. Biochem. 114 (2012) 82–93.
[44] K. Gurova, Future Oncol. 5 (2009) 1685.
[45] B.M. Zeglis, V.C. Pierre, J.K. Barton, Chem. Commun. (2007) 4565–4579.
[46] D.R. Boer, A. Canals, M, Coll, Dalton Trans, 2009, pp. 399–414.
[47] L. Strekowski, B. Wilson, Mutat. Res. 623 (2007) 3–13.
[48] L.R. Ferguson, W.A. Denny, Mutat. Res. 623 (2007) 14–23.
[49] S.S. Lucky, K.C. Soo, Y. Zhang, Chem. Rev. 115 (2015) 1990–2042.
[50] J. Marmur, J. Mol. Biol. 3 (1961) 208–211.
[51] M.F. Reichmann, S.A. Rice, C.A. Thomas, P. Doty, J. Am. Chem. Soc. 76 (1954) 3047–3053.
[52] G. Suez, V. Bloch, G. Nisnevich, M. Gandelman, Eur. J. Org. Chem. (2012) 2118–2122.
[53] Bruker Analytical X-ray Systems, Inc. Apex2, Version 2 User Manual, M86-E01078, WI, Madison, 2006.
[54] Siemens Industrial Automation, Inc, SADABS, Area-Detector Absorption Correction; Madison, WI, 1996.
[55] L. Palatinus, G. Chapuis, J. Appl. Crystallogr. 40 (2007) 786–790.
[56] P.W. Betteridge, J.R. Carruthers, R.I. Cooper, K. Prout, D.J. Watkin, J. Appl. Crystallogr. 36 (2003) 1487.
[57] D.J. Watkin, C.K. Prout, L.J. Pearce, CAMERON Program, Oxford University, UK, Chemical Crystallographic Laboratory, 1996.
[58] A. Wolfe, G. Shimer, T. Meehan, Biochemistry 26 (1987) 6392–6396.
[59] M.T. Carter, M. Rodriguez, A.J. Bard, J. Am. Chem. Soc. 111 (1989) 8901–8911.
[60] J.R. Lakowicz, Principles of Fluorescence Spectroscopy, 3rdEdn, Plenum Press, New York, 2006.
[61] G. Zhao, H. Lin, S. Zhu, H. Sun, Y. Chen, J. Inorg. Biochem. 70 (1998) 219–226.
[62] D.P. Heller, C.L. Greenstock, Biophys. Chem. 50 (1994) 305–312.
[63] A. Papastergiou, S. Perontsis, P. Gritzapis, A.E. Koumbis, M. Koffa, G. Psomas, K.C. Fylaktakidou, Photochem. Photobiol. Sci. 15 (2016) 351–360.
[64] L. Stella, A.L. Capodilupo, M. Bietti, Chem. Commun. (2008) 4744–4746.
[65] Y. Wang, H. Zhang, G. Zhang, W. Tao, S. Tang, J. Luminescence 126 (2007) 211–218.
[66] C. Kontogiorgis, D. Hadjipavlou-Litina, J. Enz. Inhib. Med. Chem. 18 (2003) 63–69.
[67] W.J. Geary, Coord. Chem. Rev. 7 (1971) 81–122.
[68] K. Nakamoto, Infrared and Raman Spectra of Inorganic and Coordination Compounds, Part B: Applications in Coordination, Organometallic, and Bioinorganic Chemistry, 6th ed., Wiley, New Jersey, 2009.
[69] P. Singla, V. Luxami, K. Paul, J. Photochem. Photobiol., B, Biology 168 (2017) 156–164.
[70] K.S. Prasad, L.S. Kumar, S. Chandan, B. Jayalakshmi, H.D. Revanasiddappa, Spectrochim. Acta Part A 81 (2011) 276–282.
[71] B.J. Hathaway, G. Wilkinson (Ed.), Comprehensive Coordination Chemistry, 5 Pergamon Press, Oxford, 1987, pp. 533–773.
[72] B.J. Hathaway, Struct. Bond. (Berlin) 14 (1973) 49–67.
[73] A.W. Addison, T.N. Rao, J. Reedijk, J. van Rijn, G.C. Verchoor, J. Chem, Soc., Dalton Trans, 1984, pp. 1349–1356.
[74] Q. Zhang, J. Liu, H. Chao, G. Xue, L. Ji, J. Inorg. Biochem. 83 (2001) 49–55.
[75] A.M. Pyle, J.P. Rehmann, R. Meshoyrer, C.V. Kumar, N.J. Turro, J.K. Barton, J. Am. Chem. Soc. 111 (1989) 3053–3063.
[76] A. Dimitrakopoulou, C. Dendrinou-Samara, A.A. Pantazaki, M. Alexiou, E. Nordlander, D.P. Kessissoglou, J. Inorg. Biochem. 102 (2008) 618–628.
[77] R.P. Sharma, S. Kumar, P. Venugopalan, V. Ferretti, A. Tarushi, G. Psomas, M. Witwicki, RSC Adv. 6 (2016) 88546–88556.
[78] A. Patra, B. Sen, S. Sarkar, A. Pandey, E. Zangrando, P. Chattopadhyay, Polyhedron 51 (2013) 156–163.
[79] J.L. Garcia-Gimenez, M. Gonzalez-Alvarez, M. Liu-Gonzalez, B. Macias, J. Borras, G. Alzuet, J. Inorg. Biochem. 103 (2000) 923–934.
[80] W.D. Wilson, L. Ratmeyer, M. Zhao, L. Strekowski, D. Boykin, Biochemistry 32 (1993) 4098–4104.
[81] X. He, D.C. Carter, Nature 358 (1992) 209–215.
[82] R.E. Olson, D.D. Christ, Ann. Rep, Med. Chem. 31 (1996) 327–336.
[83] K.A. Majorek, P.J. Porebski, A. Dayal, M.D. Zimmerman, K. Jablonska, A.J. Stewart, M. Chruszcz, W. Minor, Mol. Immunol. 52 (2012) 174–182.
[84] E.L. Gelamo, C. Silva, H. Imasato, M. Tabak, Protein Struct. Mol. Enzymol. 1594 (2002) 84–99.
[85] C. Tan, J. Liu, H. Li, W. Zheng, S. Shi, L. Chen, L. Ji, J. Inorg. Biochem. 102 (2008) 347–358.
[86] I. Petitpas, T. Grune, A.A. Bhattacharya, S. Twine, M. East, S. Curry, J. Mol. Biol. 314 (2001) 955–960.
[87] V. Rajendiran, R. Karthik, M. Palaniandavar, H. Stoeckli-Evans, V.S. Periasamy, M.A. Akbarsha, B.S. Srinag, H. Krishnamurthy, Inorg. Chem. 46 (2007) 8208–8221.
[88] G. Zhao, H. Lin, S. Zhu, H. Sun, Y. Chen, J. Inorg. Biochem. 70 (1998) 219–226.
[89] O.H. Laitinen, V.P. Hytönen, H.R. Nordlund, M.S. Kulomaa, Cell. Mol. Life Sci. 63 (2006) 2992–3017.
[90] G. Sudlow, D.J. Birkett, D.N. Wade, Mol. Pharmacol. 12 (1976) 1052–1061.
[91] N. Shahabadi, B. Bazvandi, A. Taherpour, J. Coord. Chem. 70 (2017) 3186–3198.
[92] N. Shahabadi, M. Hakimi, T. Morovati, S. Hadidi, K. Moeini, Luminescence 32 (2017) 43–50.
[93] R. Cini, G. Giorgi, A. Cinquantini, C. Rossi, M. Sabat, Inorg. Chem. 29 (1990) 5197–5200.
[94] M. Asif, Inter. J. Med. Chem. 2014 (2014) Article ID 395637.
[95] R.S. Giri, H.M. Thaker, T. Giordano, J. Williams, D. Rogers, V. Sudersanam, K.K. Vasu, Eur. J. Med. Chem. 44 (2009) 2184–2189.
[96] K. Hemalatha, K. Girija, Int. J. Pharm. Pharmaceut. Sci. 3 (2011) 103–106.
[97] M. Lazou, A.G. Hatzidimitriou, A.N. Papadopoulos, G. Psomas, J. Inorg. Biochem. 195 (2019) 101–110.
[98] F. Dimiza, M. Lazou, A.N. Papadopoulos, A.G. Hatzidimitriou, G. Psomas, J. Inorg. Biochem. 203 (2020) ID 110905.